materials

MDPI

Review

Ball Milling Innovations Advance Mg-Based Hydrogen Storage Materials Towards Practical Applications

Yaohui Xu [1,2], Yuting Li [3], Quanhui Hou [4,*], Yechen Hao [5] and Zhao Ding [3,*]

[1] Laboratory for Functional Materials, School of New Energy Materials and Chemistry, Leshan Normal University, Leshan 614000, China
[2] Leshan West Silicon Materials Photovoltaic New Energy Industry Technology Research Institute, Leshan 614000, China
[3] College of Materials Science and Engineering, National Engineering Research Center for Magnesium Alloys, National Innovation Center for Industry-Education Integration of Energy Storage Technology, Chongqing University, Chongqing 400044, China
[4] School of Automotive Engineering, Yancheng Institute of Technology, Yancheng 224051, China
[5] Department of Computer Science, Illinois Institute of Technology, Chicago, IL 60616, USA
* Correspondence: hqhdyx66@ycit.edu.cn (Q.H.); zhaoding@cqu.edu.cn (Z.D.)

Abstract: Mg-based materials have been widely studied as potential hydrogen storage media due to their high theoretical hydrogen capacity, low cost, and abundant reserves. However, the sluggish hydrogen absorption/desorption kinetics and high thermodynamic stability of Mg-based hydrides have hindered their practical application. Ball milling has emerged as a versatile and effective technique to synthesize and modify nanostructured Mg-based hydrides with enhanced hydrogen storage properties. This review provides a comprehensive summary of the state-of-the-art progress in the ball milling of Mg-based hydrogen storage materials. The synthesis mechanisms, microstructural evolution, and hydrogen storage properties of nanocrystalline and amorphous Mg-based hydrides prepared via ball milling are systematically reviewed. The effects of various catalytic additives, including transition metals, metal oxides, carbon materials, and metal halides, on the kinetics and thermodynamics of Mg-based hydrides are discussed in detail. Furthermore, the strategies for synthesizing nanocomposite Mg-based hydrides via ball milling with other hydrides, MOFs, and carbon scaffolds are highlighted, with an emphasis on the importance of nanoconfinement and interfacial effects. Finally, the challenges and future perspectives of ball-milled Mg-based hydrides for practical on-board hydrogen storage applications are outlined. This review aims to provide valuable insights and guidance for the development of advanced Mg-based hydrogen storage materials with superior performance.

Keywords: magnesium-based hydrides; ball milling; nanostructures; hydrogen storage; catalysts; nanocomposites

check for updates

Citation: Xu, Y.; Li, Y.; Hou, Q.; Hao, Y.; Ding, Z. Ball Milling Innovations Advance Mg-Based Hydrogen Storage Materials Towards Practical Applications. *Materials* **2024**, *17*, 2510. https://doi.org/10.3390/ma17112510

Academic Editor: Haralampos N. Miras

Received: 23 April 2024
Revised: 19 May 2024
Accepted: 20 May 2024
Published: 23 May 2024

Copyright: © 2024 by the authors. Licensee MDPI, Basel, Switzerland. This article is an open access article distributed under the terms and conditions of the Creative Commons Attribution (CC BY) license (https://creativecommons.org/licenses/by/4.0/).

1. Introduction

Hydrogen, as a clean and sustainable energy carrier, has attracted increasing attention for its potential to mitigate the environmental and energy crisis. Mg-based materials are promising candidates for solid-state hydrogen storage due to their high theoretical capacity (7.6 wt.% for MgH_2), low cost, and abundant reserves [1–4]. However, the high thermodynamic stability and sluggish kinetics of Mg-based hydrides have hindered their practical applications [5–7]. To address these challenges, various strategies have been developed, among which ball milling has emerged as a versatile and effective technique for the synthesis and modification of Mg-based hydrogen storage materials [8–10].

Ball milling is a solid-state processing technique that involves repeated welding, fracturing, and rewelding of powder particles in a high-energy ball mill [11]. The high-energy impacts and shear forces during milling can induce a variety of physical and

chemical changes in the materials, such as reductions in particle size, the introduction of defects, the formation of metastable phases, and enhancements in surface reactivity [12]. These microstructural and morphological changes can significantly improve the hydrogen storage properties of Mg-based materials, including their hydrogen capacity, absorption/desorption kinetics, and cycle stability [13,14]. Mechanical ball milling, as an efficient solid-state reaction method, exhibits many unique advantages in material mixing and mechanical alloying processes. Through the high-speed rotation of the ball milling media, using shear and impact forces, it achieves efficient mixing and reaction of materials, not only enhancing material uniformity but also significantly promoting chemical reactions and alloying processes between materials. This method has strong controllability, allowing precise adjustment of the final product properties by modulating the milling time, speed, and media. Compared with traditional alloying methods, mechanical ball milling does not require an external heat source, significantly saving energy and costs. Moreover, it has a wide applicability and is suitable for processing metals, ceramics, plastics, and complex alloy systems, demonstrating excellent versatility and flexibility. Mechanical ball milling also has good scalability and is suitable for both large-scale industrial production and small-scale experimental research, showing important practical application value.

In recent years, extensive research efforts have been devoted to the ball milling of Mg-based hydrogen storage materials, leading to substantial progress in understanding the underlying mechanisms and structure–property relationships. Various Mg-based hydrides, nanostructures, catalysts, and nanocomposites with enhanced hydrogen storage performance have been synthesized via ball milling [15–17]. Moreover, advanced characterization techniques and theoretical calculations have provided deep insights into the microstructural evolution and hydrogenation/dehydrogenation behaviors of the ball-milled materials [18,19].

This review aims to provide a comprehensive summary of the state-of-the-art progress in the ball milling of Mg-based hydrogen storage materials. The synthesis of Mg-based hydrides, nanostructures, and catalysts via ball milling will be systematically reviewed, with an emphasis on the effects of milling parameters and additives on the microstructure and hydrogen storage properties. The mechanisms of hydrogen absorption/desorption in the ball-milled materials will be discussed based on advanced characterization and theoretical studies. The limitations and future perspectives of ball milling in advancing Mg-based hydrogen storage materials towards practical applications will also be outlined.

2. Synthesis of Mg-Based Hydrides via Ball Milling

2.1. Mg-Based Binary Hydrides

MgH_2 is an efficient hydrogen storage material with a theoretical hydrogen storage capacity of up to 7.6 wt.%. It can be synthesized through various methods, such as hydrogenation and chemical vapor deposition, producing high-purity MgH_2. However, its high thermodynamic stability (reaction enthalpy change $\Delta H = -74.5$ kJ·mol^{-1} H_2, entropy change $\Delta S = -135$ J·K^{-1}·mol^{-1} H_2) results in a high dehydrogenation temperature (>350 °C) and slow reaction rate. The discrepancy between the actual and theoretical hydrogen storage capacity significantly limits its practical application [20]. At present, ball milling has been widely used to synthesize MgH_2 with improved hydrogen storage properties.

Ball milling under a hydrogen atmosphere has proven to be an effective strategy to mitigate particle agglomeration and oxidation issues that commonly arise during the milling process. Lu et al. [21] reported that after milling, the surface area of pure Mg exhibited a substantial increase from 0.61 m^2/g to 6.16 m^2/g, accompanied by a reduction in crystal size. The beneficial effects of milling under a hydrogen atmosphere were further demonstrated by the enhanced hydrogen storage capacity of the milled Mg powder. At 350 °C, the hydrogen storage capacity of Mg powder milled under a hydrogen atmosphere reached 3.36 wt.% H_2, a significant improvement compared to the 0.14 wt.% achieved using conventional ball milling.

The hydrogen storage properties of ball-milled MgH_2 can be further improved by optimizing the milling parameters, such as milling time, milling speed, ball-to-powder ratio, and hydrogen pressure [22]. Varin et al. [23] systematically investigated the effects of milling time on the microstructure and hydrogen storage properties of MgH_2. They found that the hydrogen desorption temperature decreased with increasing milling time, reaching a minimum of 277 °C after 20 h of milling. Prolonged milling led to the agglomeration of MgH_2 particles and the introduction of impurities, which deteriorated the hydrogen storage properties.

2.2. Mg-Based Ternary Hydrides

Ball milling has also been applied to synthesize Mg-based ternary and complex hydrides with improved thermodynamic and kinetic properties. By adding metal elements, the crystal structure can be regulated to promote the formation of new crystal phases, improving hydrogen absorption and desorption kinetics and stability. The interfacial catalytic effects of metal elements accelerate hydrogen absorption and desorption, reducing the activation energy of the reaction. It adjusts the hydrogen diffusion behavior in MgH_2, speeding up hydrogenation and dehydrogenation reactions, enhancing thermodynamic stability, lowering thermal decomposition temperatures, and extending cycle life. Mg_2CoH_5, with a hydrogen content of 4.5 wt.%, has been reported to have a lower decomposition temperature and faster kinetics than MgH_2 [24]. Apart from Mg_2CoH_5, other Mg-based binary hydrides, such as Mg_2NiH_4 and Mg_2FeH_6, have also been successfully synthesized via ball milling. Mg_2NiH_4 exhibits a higher hydrogen content of 5 wt.% and a lower decomposition temperature of 240 °C compared to Mg_2CoH_5 [25].

Complex hydrides, such as $Mg(NH_2)_2$ and $Mg(BH_4)_2$, have attracted increasing attention due to their high hydrogen contents (7.2 wt.% for $Mg(NH_2)_2$ and 14.9 wt.% for $Mg(BH_4)_2$) [26,27]. However, their high decomposition temperatures and poor reversibility have hindered their practical applications. Ball milling has been used to synthesize these complex hydrides with improved hydrogen storage properties. The ball-milled $Mg(NH_2)_2$ exhibited a hydrogen desorption temperature of 150 °C, which was 250 °C lower than that of the original $Mg(NH_2)_2$.

$Mg(BH_4)_2$ has been synthesized by ball milling a mixture of MgB_2 and $LiBH_4$ [28]. The ball-milled $Mg(BH_4)_2$ showed a hydrogen desorption temperature of 260 °C, which was 140 °C lower than that of the as-synthesized $Mg(BH_4)_2$. The improved kinetics were attributed to the reduced particle size and the formation of $LiMg(BH_4)_3$ during ball milling, which destabilized the $Mg(BH_4)_2$ structure. Table 1 summarizes the preparation methods and hydrogen storage properties of Mg-based ternary and complex hydrides. Ball milling of MgH_2 with $LiNH_2$ and $LiBH_4$ can produce $Mg(NH_2)_2$ and $Mg(BH_4)_2$, respectively. These complex hydrides have higher hydrogen capacities and lower dehydrogenation temperatures than binary hydrides. $Mg(NH_2)_2$ decomposes to $Li_2Mg(NH)_2$ during dehydrogenation, while ball milling of $Mg(BH_4)_2$ with $LiBH_4$ forms $LiMg(BH_4)_3$.

Table 1. Preparation methods and hydrogen storage properties of Mg-based ternary and complex hydrides [24–28].

Hydride	Preparation Method	Milling Time (h)	Milling Speed (rpm)	Ball-to-Powder Ratio	Hydrogen Pressure (MPa)	Dehydrogenation Temperature (°C)	Hydrogen Capacity (wt.%)	Desorption Activation Energy (kJ/mol)
Mg_2CoH_5	Ball milling of MgH_2 and Co	2	400	30:1	3.0	265	4.2	121
Mg_2NiH_4	Ball milling of MgH_2 and Mg_2Ni	3	\	30:1	1.0	240	5	\
$Mg(NH_2)_2$	Ball milling of MgH_2 and $LiNH_2$	3	300	20:1	-	150	7.2	76

Table 1. *Cont.*

Hydride	Preparation Method	Milling Time (h)	Milling Speed (rpm)	Ball-to-Powder Ratio	Hydrogen Pressure (MPa)	Dehydrogenation Temperature (°C)	Hydrogen Capacity (wt.%)	Desorption Activation Energy (kJ/mol)
$Mg(BH_4)_2$	Ball milling of MgB_2 and $LiBH_4$	1	200	10:1	0.1	260	14.9	118
$Li_2Mg(NH)_2$	Decomposition of $Mg(NH_2)_2$	-	-	-	-	150	5.6	54
$LiMg(BH_4)_3$	Ball milling of $Mg(BH_4)_2$ and $LiBH_4$	2	250	15:1	0.1	180	11.5	92

2.3. Mechanisms of Mg-Based Hydride Formation during Ball Milling

The formation of Mg-based hydrides during ball milling involves a series of physical and chemical processes, including particle refinement, surface activation, and chemical reactions [29]. The high-energy impacts during ball milling can effectively reduce the particle size and create fresh surfaces, which facilitate the diffusion and dissociation of hydrogen molecules. The accumulation of defects and strain energy during milling also enhances the reactivity of the Mg-based materials towards hydrogen [30].

The formation mechanism of MgH_2 during ball milling under a hydrogen atmosphere has been extensively studied. Czujko et al. [31] proposed a three-stage mechanism for the formation of MgH_2 during ball milling: (i) refinement of Mg particles and creation of fresh surfaces; (ii) chemisorption of hydrogen on the Mg surfaces and nucleation of MgH_2; (iii) growth of MgH_2 phase and further refinement of the particles. The rate-limiting step is the nucleation of MgH_2, which requires a critical hydrogen pressure and a sufficient number of active sites on the Mg surfaces.

For Mg-based binary and ternary hydrides, the formation mechanism during ball milling involves the interdiffusion and reaction of the constituent elements under a hydrogen atmosphere. The high-energy impacts can induce the formation of metastable phases and enhance the atomic diffusion, which facilitate the formation of the hydride phases [32]. For example, during the ball milling of Mg and Ni powders under a hydrogen atmosphere, the formation of Mg_2NiH_4 involves the following steps: (i) formation of Mg_2Ni alloy; (ii) hydrogenation of Mg_2Ni to form $Mg_2NiH_{0.3}$; (iii) disproportionation of $Mg_2NiH_{0.3}$ into MgH_2 and Mg_2NiH_4.

The formation of Mg-based complex hydrides during ball milling involves the solid-state reaction between MgH_2 and the complex hydride precursors (e.g., $LiNH_2$, $LiBH_4$). The high-energy impacts can break the B-H and N-H bonds in the complex hydrides and facilitate the exchange of H atoms with MgH_2, leading to the formation of $Mg(NH_2)_2$ and $Mg(BH_4)_2$ [33]. The simultaneous refinement of the particles and mixing of the reactants also enhance the contact area and reactivity, which promote the solid-state reactions.

3. Nanostructuring of Mg-Based Hydrides via Ball Milling

Nanostructuring has been recognized as an effective strategy to improve the hydrogen storage properties of Mg-based hydrides [34]. Nanostructured materials have a high surface-to-volume ratio, short diffusion paths, and a large number of grain boundaries and defects, which can enhance the hydrogen absorption/desorption kinetics and reduce the thermal stability [35]. Ball milling is a simple and efficient technique to produce nanostructured Mg-based hydrides with a high yield and low cost.

3.1. Nanocrystalline Mg-Based Hydrides

The reversible reaction of hydrogen with metal Mg to form MgH_2 has special properties for energy storage. However, the high thermodynamic stability of the hydride results in high absorption/desorption temperatures. Nanocrystalline Mg-based hydrides have been extensively studied for hydrogen storage applications. Modifying processing routes or combinatorial routes can also lead to refined microstructures, including methods such

as melt spinning, cold rolling, and mechanical milling, which can be used to prepare nanocrystalline MgH_2 structures.

As the particle size is reduced below a critical value, a remarkable decrease in the desorption temperature is observed. Specifically, when the particle size is reduced to the range of 500–600 nm, the onset desorption temperature of MgH_2 exhibits a substantial reduction of approximately 40–60 °C. Microstructural analysis of MgH_2 powder subjected to ball milling for durations exceeding 10 h reveals the coexistence of metastable γ-MgH_2 and stable nanocrystalline β-MgH_2 phases. Quantitative evidence suggests that the refinement of powder granularity and the presence of the γ-MgH_2 phase within the particles are the primary factors contributing to the significant reduction in the desorption temperature of MgH_2 hydride [36].

MgH_2 nanowires exhibit significantly lower desorption barriers (33.5 and 38.8 kJ mol^{-1} for hydrogenation and dehydrogenation, respectively) compared to commercial MgH_2 (120–142 kJ·mol^{-1}). Table 2 summarizes the preparation conditions and hydrogen storage properties of nanocrystalline Mg-based hydrides. Theoretical predictions suggest that reducing the diameter of the nanowires below 30 nm can substantially influence the thermodynamics and kinetics of MgH_2 [37]. Furthermore, experimental investigations on the hydrogen storage performance of MgH_2 with varying particle sizes (25, 32, 38 nm) provide compelling evidence that smaller particle sizes lead to enhanced hydrogenation kinetics [38].

Table 2. Preparation conditions and hydrogen storage properties of nanocrystalline Mg-based hydrides [36–38].

Hydride	Composition	Milling Time (h)	Milling Speed (rpm)	Ball-to-Powder ratio	Hydrogen Pressure (MPa)	Grain Size (nm)	Dehydrogenation Temperature (°C)	Activation Energy (kJ/mol)	Hydrogen Capacity (wt.%)	Reversible Capacity (wt.%)
MgH_2	MgH_2	20	400	10:1	1.0	5–10	200	76	7.2	6.8
Mg_2NiH_4	Mg_2Ni + MgH_2	25	300	20:1	3.0	3–5	200	87	3.0	2.8
MgH_2	MgH_2 + 10 wt.% LiH	1	200	10:1	1.0	7	150	65	6.0	5.8
MgH_2	MgH_2 + 5 wt.% Nb_2O_5	20	400	30:1	1.0	5–10	200	61	6.5	6.2
Mg_2NiH_4	Mg_2Ni + 10 wt.% TiH_2	30	250	40:1	3.0	10–20	220	85	3.5	3.2

3.2. Amorphous Mg-Based Hydrides

Amorphous Mg-based hydrides have also been synthesized via ball milling and have shown improved hydrogen storage properties compared to their crystalline counterparts. Unlike crystalline materials, amorphous hydrides lack long-range atomic order and have a high density of defects and free volume, which can facilitate hydrogen diffusion and reduce the stability of the hydrides [39–41].

Zhang et al. [42] synthesized amorphous $CeMg_{11}Ni$ alloys with varying Ni contents (x wt.% Ni, where x = 100, 200) via ball milling. The degree of amorphization of the alloy was found to increase with increasing Ni contents. The hydrogen storage capacities of the alloys with x = 100 and x = 200 were determined to be 5.94 wt.% and 6.15 wt.%, respectively. Moreover, the dehydrogenation rate exhibited a consistent increase with increasing Ni contents.

Liang et al. [43] successfully synthesized an amorphous La@Mg compound by ball milling a mixture of ($La(acac)_3$) and Mg. This composite material exhibited a remarkable hydrogen storage capacity of approximately 7.6% and a hydrogen desorption rate of 7.2%, surpassing the performance of its crystalline La@Mg counterpart and pure Mg. The adsorption/desorption kinetics were rapid, and the reversible adsorption/desorption cycles demonstrated excellent stability. Theoretical calculations in conjunction with experimental results revealed that the amorphous La@Mg structure provides channels for enhanced hydrogen diffusion. This unique feature facilitates the hydrogenation process by accelerating the diffusion of H atoms between the subsurface and surface regions. Table 3

summarizes the preparation conditions and hydrogen storage properties of amorphous Mg-based hydrides. Long-time high-energy ball milling with the addition of alloying elements can produce amorphous MgH_2 and Mg_2NiH_4. Amorphous hydrides exhibit better hydrogen storage kinetics than their crystalline counterparts due to the increased defects and free volume. The addition of TiF_3 and VTiCr can further improve the amorphization and hydrogen storage properties of MgH_2 and Mg_2NiH_4.

Table 3. Preparation conditions and hydrogen storage properties of amorphous Mg-based hydrides [39–43].

Hydride	Composition	Milling Time (h)	Milling Speed (rpm)	Ball-to-Powder Ratio	Hydrogen Pressure (MPa)	Dehydrogenation Temperature (°C)	Dehydrogenation Activation Energy (kJ/mol)	Hydrogen Capacity (wt.%)	Reversible Capacity (wt.%)
MgH_2	MgH_2 + 10 wt.% Ni	20	400	30:1	1.0	150	72	6.8	6.5
Mg_2NiH_4	$Mg_2Ni + MgH_2$	100	200	50:1	3.0	200	98	3.0	2.8
Mg-Ni-Y	$Mg_{65}Ni_{30}Y_5$	20	300	40:1	3.0	200	105	3.5	3.2
Mg_2NiH_4	Mg_2Ni + 5 wt.% TiF_3	50	250	60:1	3.0	180	84	3.2	3.0
MgH_2	MgH_2 + 10 wt.% VTiCr	10	500	20:1	1.0	120	63	6.0	5.5

3.3. Mechanisms of Nanostructure/Amorphous Formation during Ball Milling

The formation of nanostructures during ball milling involves a series of physical and chemical processes, including particle refinement, strain accumulation, and phase transformation [44]. Figure 1a illustrates the preparation process, where high-energy collisions during ball milling effectively reduce the particle size and introduce a high density of defects and strain energy into the materials [45].

The formation mechanism of nanocrystalline structures during ball milling has been extensively studied. As depicted in Figure 1b, the high-energy impacts during ball milling lead to repeated particle deformation, fractures, and welding, resulting in a significant reduction in particle size and a concomitant increase in surface area [46]. Fecht [47] proposed a three-stage model for the formation of nanocrystalline structures during ball milling: (i) initial stage: refinement of particles and introduction of defects; (ii) intermediate stage: formation of nanocrystalline domains and grain boundaries; (iii) final stage: further refinement of nanocrystalline domains and saturation of grain size. The final grain size is determined by the balance between the plastic deformation and dynamic recovery during ball milling.

The formation of amorphous structures during ball milling involves the accumulation of strain energy and the suppression of crystallization [48]. When the strain energy stored in the materials reaches a critical value, the crystalline structure becomes unstable and transforms into an amorphous state. The critical strain energy depends on the nature of the materials and the milling conditions. For Mg-based hydrides, the formation of amorphous structures is favored by the presence of additives (e.g., Ni, Y) and the high energy input during ball milling [49]. Figure 1c reveals the evolution of the microstructure during the milling process. As the milling progresses, amorphous phases gradually nucleate and grow at the expense of the crystalline phases due to the accumulation of strain energy. The crystalline domains continuously shrink and ultimately disappear, resulting in a fully amorphous structure [50].

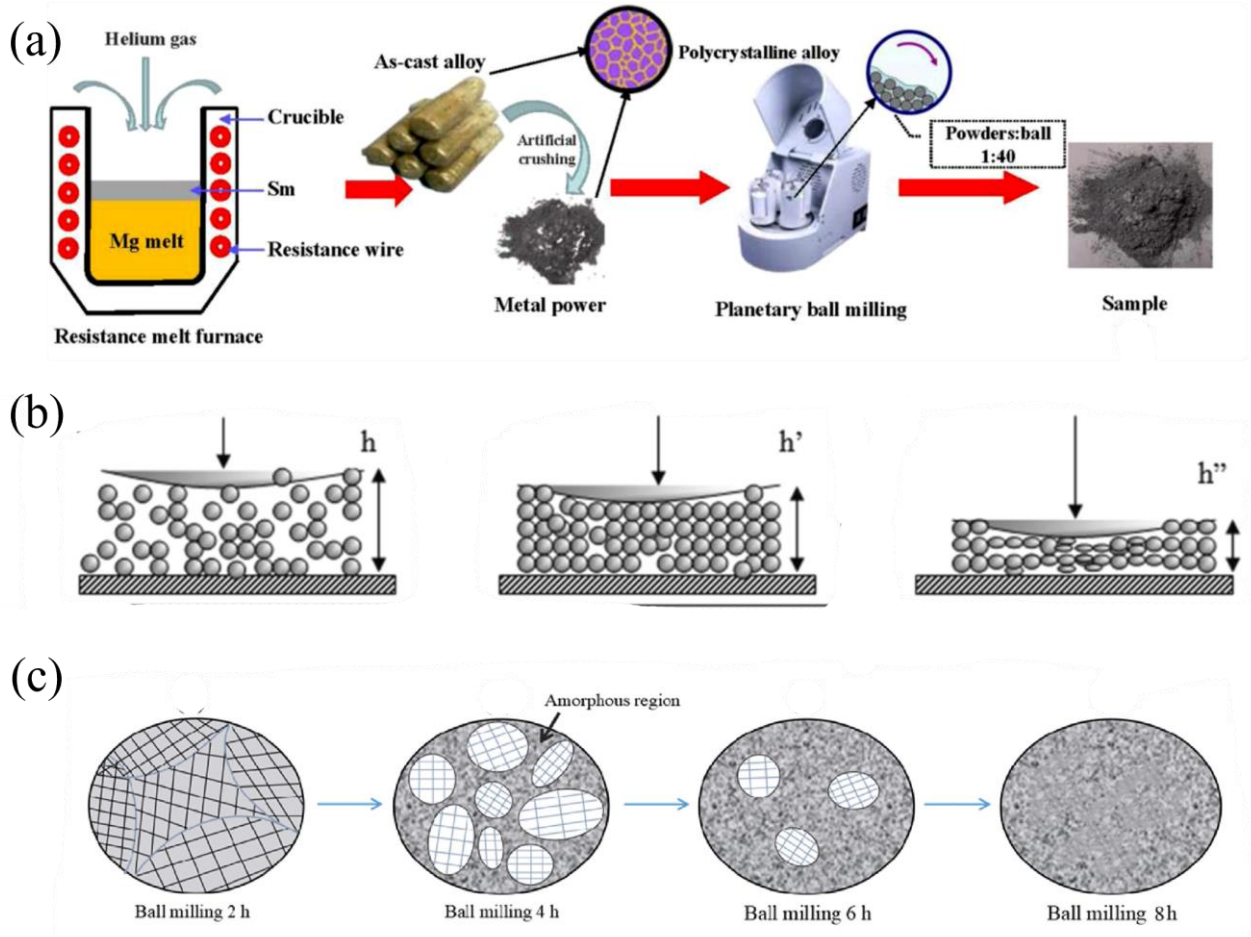


Figure 1. (**a**) Flowchart for the preparation method of the as-milled Sm_5Mg4_1 alloy [45]. (**b**) Illustration of the deformation of powder agglomerate during the impact process [46]. (**c**) Illustration of the different microstructural states of the Mg_2Ni alloys [50].

The formation of nanostructures during the ball milling process is influenced by several factors, including the hydrogen pressure and the presence of additives. Cuevas et al. [51] successfully synthesized MgH_2-TiH_2 nanocomposites with grain sizes ranging from 4 to 12 nm through reactive ball milling under a hydrogen pressure of 8 MPa. The catalytic properties of TiH_2 played a crucial role in accelerating the formation of the MgH_2 phase, enabling the nanocomposite to form within a remarkably short duration of less than 50 min. Furthermore, the TiH_2 phase effectively inhibited the coarsening of Mg grains, allowing the MgH_2 phase to nucleate and subsequently form a continuous hydride layer within the Mg nanoparticles.

4. Catalytic Modification of Mg-Based Hydrides via Ball Milling

Catalytic modification has been widely used to enhance the hydrogen storage properties of Mg-based hydrides [52]. The addition of catalysts can lower the activation energy for hydrogen absorption/desorption, increase the reaction kinetics, and improve the reversibility and cycling stability of the hydrides [53]. Ball milling is an effective technique to introduce catalysts into Mg-based hydrides and achieve a uniform distribution and strong interaction between the catalysts and the hydrides [54].

4.1. Transition Metal Catalysts

Transition metals, such as Ti, V, Mn, Fe, Co, Ni, Cu, and Nb, have been extensively studied as catalysts for Mg-based hydrides [55]. These metals have a high catalytic activity for hydrogen dissociation and recombination and can form stable hydrides with a high

hydrogen storage capacity [56]. The catalytic effects of transition metals on the hydrogen storage properties of Mg-based hydrides have been attributed to several mechanisms, including the spillover effect, the gateway effect, and the hydride-forming effect [57–59].

Liang et al. [60] investigated the catalytic effects of different transition metals (Ti, V, Mn, Fe, Ni) on the hydrogen storage properties of MgH_2. They found that the addition of 1 mol% of transition metals via ball milling significantly reduced the dehydrogenation temperature and activation energy of MgH_2. Composites with Ti or V added exhibit rapid desorption kinetics above 250 °C and rapid adsorption kinetics below 25 °C. The enhanced catalytic effect of Ti and V was attributed to their strong interaction with MgH_2 and the formation of stable hydrides (TiH_2 and VH_2) during dehydrogenation.

Wu et al. [61] facilitated the ball milling of Nb and MgH_2 using surfactants. The MgH_2-5 wt.% Nb composite material began releasing hydrogen at 186.7 °C, with a maximum release of 7.0 wt.%. It released 4.2 wt.% H_2 within 14 min at 250 °C and could absorb 4.0 wt.% H_2 within 30 min, even at the low temperature of 100 °C. The desorption activation energy and hydrogenation activation energy were reduced from 140.51 ± 4.74 and 70.67 ± 2.07 kJ·mol^{-1} to 90.04 ± 2.83 and 53.46 ± 3.33 kJ·mol^{-1}, respectively.

The catalytic effects of transition metals on the hydrogen storage properties of Mg-based hydrides can be further enhanced by optimizing the ball milling conditions and the catalyst composition. Lu et al. [62] successfully synthesized a MgH_2-0.1TiH_2 nanocomposite system with exceptionally fine nanocrystalline grain sizes ranging from 5 to 10 nm. This was achieved through an innovative ultra-high-energy-high-pressure mechanical milling approach. The TiH_2 phase was homogeneously dispersed among the MgH_2 particles, forming a well-distributed nanocomposite. The synergistic effects of the nanoscale structure and the catalytic influence of TiH_2 led to a remarkable enhancement in the dehydrogenation and hydrogenation kinetics of the MgH_2-0.1TiH_2 system compared to commercial MgH_2.

Cui et al. [63] developed an innovative approach to enhance the catalytic effects of Ti on MgH_2 by coating ball-milled Mg powder (approx. 1 μm in diameter) with a multivalent Ti-based catalyst. The coating process involved a chemical reaction between the Mg powder and $TiCl_3$ in a THF solution, resulting in the formation of a 10 nm thick catalyst layer. This layer contained multiple valence states of Ti, including Ti, TiH_2, $TiCl_3$, and TiO_2. The presence of these diverse Ti valence states played a crucial role in facilitating electron transfer between Mg^{2+} and H^-, thereby promoting the recombination of H_2 on the Ti surface. The resulting MgH_2-encapsulated Ti-based system (Mg-Ti) demonstrated a remarkable dehydrogenation performance, with hydrogen release initiating at around 175 °C and achieving a release of 5 wt.% H_2 within a mere 15 min at 250 °C.

Table 4 summarizes the effects of transition metal catalysts on the hydrogen storage properties of Mg-based hydrides. The addition of Ti, V, Mn, Fe, Ni, Nb, and their alloys via ball milling can significantly improve the hydrogen storage kinetics of MgH_2 and Mg_2NiH_4. Ti and V show the best catalytic effects, while the catalytic effects of Mn, Fe, and Ni are relatively weak. The catalytic effects depend on the catalyst composition, milling time, and milling parameters.

Table 4. Effects of transition metal catalysts on the hydrogen storage properties of Mg-based hydrides [56–63].

Hydride	Catalyst (mol%)	Milling Time (h)	Milling Speed (rpm)	Ball-to-Powder Ratio	Dehydrogenation Temperature (°C)	Activation Energy (kJ/mol)	Hydrogen Capacity (wt.%)	Reversible Capacity (wt.%)
MgH_2	1% Ti, V, Mn, Fe, Ni	1	400	10:1	250 (Ti, V), 300 (Mn, Fe, Ni)	61 (Ti, V), 92 (Mn, Fe, Ni)	6.5 (Ti, V), 6.0 (Mn, Fe, Ni)	6.2 (Ti, V), 5.8 (Mn, Fe, Ni)
MgH_2	1% Nb	2	500	20:1	200	61	6.8	6.5
MgH_2	10% Ni	0.5–5	300	30:1	250 (5 h)	67 (5 h)	6.2 (5 h)	6.0 (5 h)
MgH_2	Ti-Fe-Nb (1:1:1)	2	400	40:1	150	53	6.5	6.2
MgH_2	5% VTiCr	10	500	20:1	180	59	6.0	5.8
Mg_2NiH_4	10% TiH_2	30	250	60:1	220	85	3.5	3.2

4.2. Metal Oxide Catalysts

Metal oxides such as Nb_2O_5, TiO_2, V_2O_5, Cr_2O_3, and Al_2O_3 have also been studied as catalysts for Mg-based hydrides [64]. These oxides have a high chemical stability and a strong interaction with hydrides, and they can act as dispersants and grain growth inhibitors during ball milling [65]. The catalytic effects of metal oxides on the hydrogen storage properties of Mg-based hydrides have been attributed to several mechanisms, including the formation of active species, the creation of hydrogen diffusion channels, and the modification of the electronic structure of the hydrides [66].

Barkhordarian et al. [67] investigated the catalytic effects of Nb_2O_5 on the hydrogen storage properties of MgH_2. By ball milling 0.5 mol.% Nb_2O_5 with MgH_2, they observed a significant enhancement in the reaction kinetics of the composite. The catalytic influence of Nb_2O_5 was particularly evident at elevated temperatures. At 300 °C, the composite exhibited rapid hydrogen release, achieving a 7 wt.% H_2 release within a mere 90 s. Similarly, the composite demonstrated fast hydrogen absorption, with 7 wt.% H_2 being absorbed within just 60 s at the same temperature. Even at a lower temperature of 250 °C, the composite showcased impressive kinetics, absorbing over 6 wt.% H_2 within 60 s and subsequently releasing it within 500 s.

Polanski et al. [68] explored the catalytic effects of nanocrystalline Cr_2O_3 on the hydrogen storage properties of MgH_2. Interestingly, they discovered that the addition of Cr_2O_3 did not significantly influence the grain size of β-MgH_2. However, despite the lack of grain size reduction, the presence of Cr_2O_3 had a profound impact on the reaction kinetics of the composite. The MgH_2-Cr_2O_3 composite exhibited remarkable hydrogen absorption and desorption rates. At 300 °C and a hydrogen pressure of 1 MPa, the composite could absorb 6 wt.% H_2 within an impressively short duration of 2 min. Moreover, under the same temperature conditions, the composite demonstrated rapid hydrogen release, achieving a 6 wt.% H_2 release within just 10 min.

The catalytic effects of metal oxides on the hydrogen storage properties of Mg-based hydrides can be further enhanced by optimizing the ball milling conditions and the catalyst morphology. Ma et al. [69] conducted a comprehensive study on the influence of catalyst morphology on the hydrogen storage properties of MgH_2. They discovered that the morphology of the catalyst played a crucial role in determining its surface energy and chemical interactions with Mg and hydrogen. To investigate this effect, they synthesized anatase TiO_2 with different crystal face advantages using a hydrothermal method. These TiO_2 catalysts, denoted as TF_x (x = 0, 10, 30, 50, 70, and 80), were then incorporated into MgH_2 via ball milling. Among the prepared composites, MgH_2-TF_{70} exhibited the most promising hydrogen adsorption kinetics, with an exceptionally low apparent activation energy for dehydrogenation of only 76.1 ± 1.6 kJ mol^{-1}. This composite material demonstrated an initial hydrogen release temperature of approximately 220 °C. Furthermore, it showcased rapid hydrogen absorption and desorption capabilities, absorbing 5.3 wt.% H_2 within a remarkable 44 s at 200 °C and releasing 6.4 wt.% H_2 within 700 s at 300 °C.

Table 5 summarizes the effects of metal oxide catalysts on the hydrogen storage properties of Mg-based hydrides. The addition of Nb_2O_5, TiO_2, Cr_2O_3, and V_2O_5 via ball milling can improve the hydrogen storage kinetics of MgH_2. The catalytic effects of metal oxides are relatively weaker than those of transition metals, but they can be enhanced by optimizing the milling conditions. The milling atmosphere, milling time, and milling parameters have significant effects on the catalytic activity and stability of metal oxides.

Table 5. Effects of metal oxide catalysts on the hydrogen storage properties of Mg-based hydrides [65–69].

Hydride	Catalyst (mol%)	Milling Atmosphere	Milling Time (h)	Milling Speed (rpm)	Ball-to-Powder Ratio	Dehydrogenation Temperature (°C)	Activation Energy (kJ/mol)	Hydrogen Capacity (wt.%)	Reversible Capacity (wt.%)
Mgh_2	0.5% Nb_2O_5	Ar	20	400	30:1	250	85	6.5	6.2
MgH_2	1% TiO_2 nanoparticles	Ar	10	500	20:1	275	96	6.2	6.0
MgH_2	1% Cr_2O_3	H_2	5	400	40:1	225	75	6.8	6.5
MgH_2	TiO_2 nanotubes (5%)	Ar	20	300	50:1	250	81	6.5	6.2
MgH_2	2% Nb_2O_5	H_2	10	500	20:1	225	68	7.0	6.8
MgH_2	5% V_2O_5	Ar	30	200	60:1	240	78	6.0	5.8

4.3. Mechanisms of Catalytic Effects during Ball Milling

The catalytic effects of transition metals and metal oxides on the hydrogen storage properties of Mg-based hydrides involve a series of physical and chemical processes during ball milling and hydrogen absorption/desorption cycles [70]. The high-energy impacts during ball milling can induce the refinement and uniform distribution of the catalysts in the hydride matrix, creating a large number of catalyst–hydride interfaces and active sites for hydrogen storage [71]. The catalysts can also act as dispersants and grain growth inhibitors, preventing the agglomeration and coarsening of the hydride particles during prolonged milling and cycling [72].

During the hydrogen absorption/desorption processes, the catalysts can facilitate the dissociation and recombination of hydrogen molecules on the surface of the hydrides, lowering the activation energy and increasing the reaction rates [73]. The dissociated hydrogen atoms can migrate from the catalyst surface to the hydride surface via the spillover effect and then diffuse into the bulk of the hydride via the gateway effect [74]. The presence of catalysts can also modify the electronic structure of the hydrides, weakening the Mg-H bonds and facilitating hydrogen desorption [75].

The specific catalytic mechanisms depend on the nature of the catalysts and the hydrides, as well as the reaction conditions. For transition metal catalysts, the formation of stable hydrides (e.g., TiH_2, VH_2, $NbH_{0.89}$) during the hydrogen absorption/desorption cycles can provide additional catalytic sites and hydrogen diffusion channels, enhancing the overall kinetics [76]. For metal oxide catalysts, the reduction of the oxides to lower valence states or metallic phases during the hydrogen absorption/desorption cycles can create active species and defects, which facilitate the hydrogen storage reactions [77].

The catalytic mechanisms can also involve the formation of intermediate phases and solid solutions during the hydrogen absorption/desorption cycles. For example, the addition of Fe to MgH_2 can lead to the formation of the Mg_2FeH_6 intermediate phase during hydrogen absorption, which enhances the hydrogen diffusion and storage capacity [78]. The addition of Nb to MgH_2 can lead to the formation of a Mg-Nb solid solution during dehydrogenation, which improves the reversibility and cycling stability of the hydride [79].

To elucidate the catalytic mechanisms of transition metals, we take Ni as a representative example. Figure 2a presents micron-sized Ni-encapsulated MgH_2 composite materials with an average particle size ranging from 2 to 10 μm, where the Ni particles exhibit a size comparable to that of MgH_2 [80]. In contrast, Figure 2b showcases MgH_2-nNi (2 h) samples, revealing nanoscale Ni particles encapsulating MgH_2 with an average particle size of 1–5 μm. Compared to pure MgH_2, the incorporation of Ni via doping leads to the partial substitution of Mg atoms, resulting in an increased overlap of electron clouds (Figure 2c) [81]. This phenomenon indicates the formation of stronger covalent interactions between Mg and Ni atoms, which consequently weakens the Mg-H bond strength. As a result, the kinetics of hydrogen absorption and desorption reactions in the Ni-doped MgH_2 composite material are significantly enhanced [81].

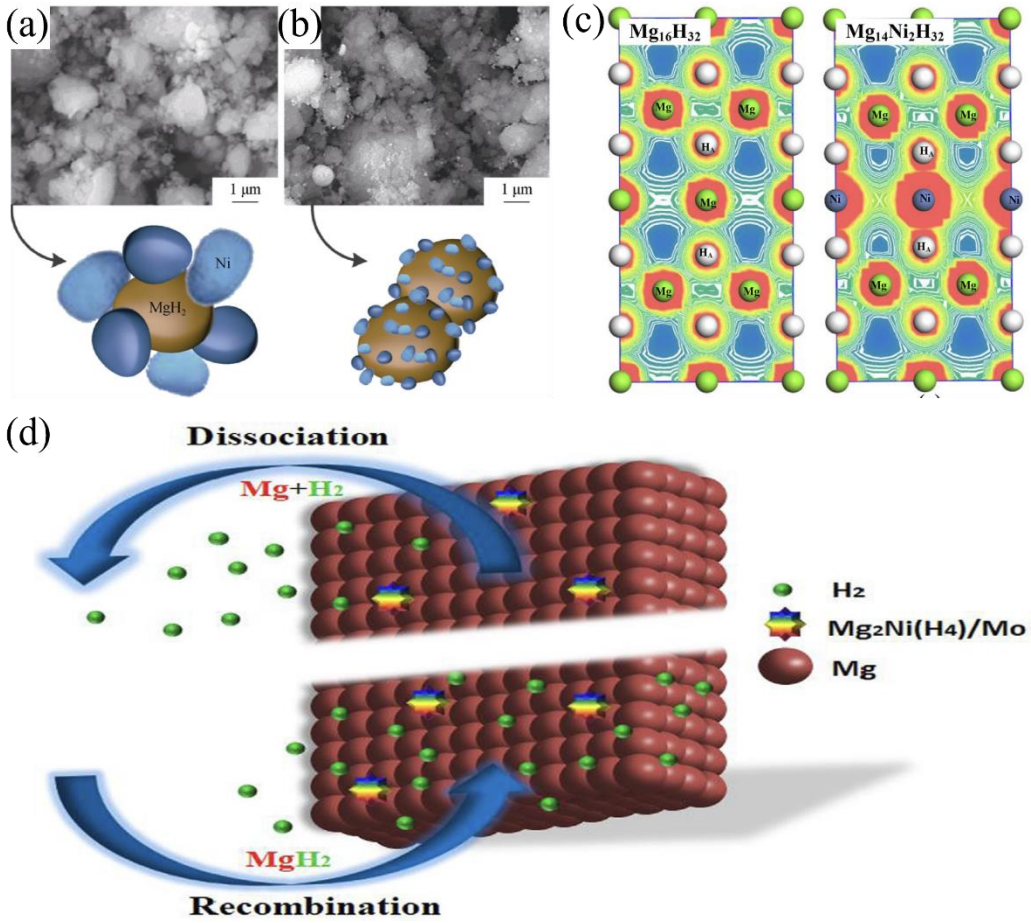


Figure 2. SEM images and schematic models of samples: (**a**) MgH_2-mNi (2 h); (**b**) MgH_2-nNi (2 h) [80]; (**c**) total charge densities in (110) crystal planes of $Mg_{16}H_{32}$,$Mg_{14}Ni_2H_{32}$ [81]; (**d**) schematic diagram of the de/re-hydrogenation processes of the MgH_2 + NiO@$NiMoO_4$ composite [82].

In the case of metal oxides, the in situ formation of catalytically active alloy phases during the hydrogen absorption and desorption processes plays a pivotal role in enhancing the hydrogen storage performance of Mg-based hydrides. Figure 2d illustrates the catalytic mechanism of NiO/$NiMoO_4$-doped MgH_2 composite materials. During the hydrogen absorption and desorption processes, the composite undergoes an in situ formation of catalytically active Mg_2Ni/Mg_2NiH_4 and Mo phases. These newly formed species play a crucial role in accelerating the dissociation of H_2 molecules on the surface of MgH_2. Moreover, they create a "hydrogen pump" effect, facilitating the reversible hydrogen absorption and desorption in MgH_2 under relatively mild conditions [82].

The optimization of the catalytic effects requires a comprehensive understanding of the structure–property relationships and the reaction mechanisms of the catalyst–hydride systems. Advanced characterization techniques such as X-ray diffraction (XRD), transmission electron microscopy (TEM), X-ray photoelectron spectroscopy (XPS), and neutron scattering have been used to investigate the microstructure, morphology, electronic structure, and hydrogen storage properties of ball-milled Mg-based hydrides with catalysts. Theoretical calculations such as density functional theory (DFT) and molecular dynamics (MD) simulations have also been used to predict the catalytic activity and the hydrogen storage mechanisms of the catalyst–hydride systems.

5. Nanocomposite Mg-Based Hydrides via Ball Milling

Nanocomposite Mg-based hydrides, consisting of nanosized Mg-based hydrides and other functional materials (e.g., carbon materials, metal hydrides, metal organic frame-

works), have attracted increasing attention for hydrogen storage applications [83]. The incorporation of functional materials into the Mg-based hydrides can create synergistic effects, such as improved thermal conductivity, enhanced hydrogen diffusion, and reduced hydride stability, leading to superior hydrogen storage properties [84]. Ball milling is a simple and effective technique to prepare nanocomposite Mg-based hydrides with a uniform distribution and strong interaction between the components.

5.1. Carbon-Containing Nanocomposites

Carbon materials, such as graphite, carbon nanotubes (CNTs), and graphene, have been widely used to prepare nanocomposite Mg-based hydrides due to their high thermal conductivity, high surface area, and excellent mechanical properties [85]. The addition of carbon materials to Mg-based hydrides via ball milling can enhance the thermal management and hydrogen diffusion of the system, leading to improved hydrogen absorption/desorption kinetics and reversibility [86].

Pal et al. [87] reported a significant reduction in the dehydrogenation temperature of MgH_2 by ball milling with 10 wt.% flake graphene. The dehydrogenation temperature decreased from 410 °C for pure MgH_2 to 282 °C for the MgH_2–graphene composite. This reduction in temperature is noteworthy, as it is substantially lower than the dehydrogenation temperature of pure MgH_2. The incorporation of graphene also led to a decrease in the dehydrogenation activation energy from 170 kJ/mol for pure MgH_2 to 136 ± 2 kJ/mol for the composite. Interestingly, XRD analysis before and after the dehydrogenation reaction confirmed the presence of graphene, indicating that no direct chemical reaction occurred between graphene and MgH_2.

Rather et al. [88] investigated the hydrogen storage properties of ball-milled MgH_2 with 5 wt.% carbon nanotubes (CNTs) and observed a hydrogen absorption capacity of 5.5 wt.% under a hydrogen pressure of 4.6 MPa at 673 K. Kinetic rate modeling studies provided valuable insights into the role of CNTs in enhancing hydrogen storage performance. The results indicated that CNTs facilitate the diffusion of hydrogen within the Mg matrix, thereby accelerating the formation of the hydride phase. Furthermore, the interaction between Mg and C atoms created abundant sites for hydrogen dissociation and diffusion. The unique tubular structure of CNTs also contributed to improved internal H_2 transport within the composite material.

Peng et al. [89] synthesized a novel MgH_2@CA microsphere composite material by ball milling carbon aerogel (CA) microspheres, which possessed a mesh-like internal structure, with Mg powder followed by an activation process. The resulting composite exhibited a distinctive core–shell structure that significantly enhanced the hydrogenation and dehydrogenation rates. The composite material demonstrated rapid hydrogen absorption, achieving a capacity of 6.2 wt.% H_2 within a mere 5 min at 275 °C. Additionally, it exhibited fast hydrogen release, liberating 4.9 wt.% H_2 within 100 min at 350 °C. The apparent activation energy for dehydrogenation was remarkably reduced to 114.8 kJ/mol. These improvements were attributed to the in situ-formed MgH_2 nanoparticles, which reduced the diffusion distance of H_2, and the CA matrix, which provided nucleation sites and prevented particle agglomeration.

Table 6 summarizes the effects of carbon materials on the hydrogen storage properties of Mg-based hydride nanocomposites. The addition of graphite, carbon nanotubes (CNTs), graphene, and fullerene (C60) via ball milling can significantly improve the hydrogen storage kinetics of MgH_2 and Mg_2NiH_4. The catalytic effects of carbon materials depend on their morphology, size, structure, and content. Carbon materials can enhance the thermal conductivity, facilitate the hydrogen diffusion, and prevent the particle aggregation of Mg-based hydrides.

Table 6. Effects of carbon materials on the hydrogen storage properties of Mg-based hydride nanocomposites [85–89].

Hydride	Carbon Additive (wt.%)	Milling Time (h)	Milling Speed (rpm)	Ball-to-Powder Ratio	Dehydrogenation Temperature (°C)	Activation Energy (kJ/mol)	Hydrogen Capacity (wt.%)	Reversible Capacity (wt.%)
MgH_2	5% graphite	10	400	30:1	300	108	6.5	6.2
MgH_2	10% CNTs	2	500	20:1	275	102	6.0	5.8
MgH_2	5% graphene	5	400	40:1	250	91	6.5	6.3
MgH_2	2% C60	10	300	50:1	265	97	6.8	6.5
Mg_2NiH_4	10% CNTs	25	200	60:1	220	83	3.2	3.0

5.2. Metal Hydride-Containing Nanocomposites

Metal hydrides such as $LiBH_4$, $NaAlH_4$, and TiH_2 have been used to prepare nanocomposite Mg-based hydrides due to their high hydrogen storage capacity and catalytic effects [90,91]. The addition of metal hydrides to Mg-based hydrides via ball milling can create hydrogen diffusion channels and active sites, leading to enhanced hydrogen absorption/desorption kinetics and reversibility [92].

Ding et al. [93] further advanced the ball milling approach by introducing $LiBH_4$ nanoparticles in aerosol form (Figure 3a), which resulted in the formation of MgH_2-$LiBH_4$ composite materials with a superior hydrogen release performance. Figure 3b reveals the hydrogen release mechanism in pristine MgH_2, where the contraction of the MgH_2 core during dehydrogenation leads to the formation of a continuous Mg shell. This Mg shell acts as a barrier, hindering the decomposition of MgH_2 and the diffusion of H_2 molecules. However, the introduction of $LiBH_4$ nanoparticles alters the reaction pathway (Figure 3c). At the Mg/$LiBH_4$ interface, new reactions take place, resulting in the formation of MgB_2 and LiH. These interfacial reactions effectively break the Mg shell surrounding MgH_2, thus promoting the release of H_2.

Kwak et al. [94] employed reactive ball milling to synthesize MgH_2-$NaAlH_4$ composite materials with varying ratios. As the $NaAlH_4$ content increased, a notable trend was observed in the curve depicting the ratio of hydrogen release at the temperature peak to the increase in temperature. The composite with the composition MgH_2-30$NaAlH_4$ demonstrated the most promising performance among the prepared samples. This composite exhibited a remarkable hydrogen absorption capacity of 7.42 wt.% within a short duration of 10 min at 320 °C. Moreover, it showcased rapid hydrogen release, liberating the same amount of H within an impressive timeframe of just 20 min at the same temperature.

El-Eskandarany et al. [95] successfully synthesized MgH_2-5.3 wt.%TiH_2 composite material via reactive ball milling. The composite exhibited impressive hydrogen storage properties at relatively low temperatures. At 175 °C, the material adsorbed 5.5 wt.% H_2 within a short duration of 6 min. Similarly, at 250 °C, it released the same amount of H_2 within just 7 min. Furthermore, the synthesized nanocomposite powder demonstrated remarkable cyclic stability, maintaining its performance for an extended cycle life of up to 580 h without any observable decay.

The improved hydrogen storage properties were attributed to the catalytic effects of the Ti phase formed during the dehydrogenation of TiH_2, which acted as a gateway for hydrogen diffusion and a seed for the nucleation of MgH_2. Figure 3d illustrates the catalytic principle of TiH_2 in the Mg_2NiH_4 system. The in situ-formed Ti-H species interact synergistically with Mg_2Ni, creating additional active sites for hydrogen dissociation and recombination on the MgH_2 surface. Moreover, these Ti-H species facilitate the diffusion and migration of atomic and molecular hydrogen through a "hydrogen pump" effect, which further enhances the hydrogen absorption and desorption kinetics [96].

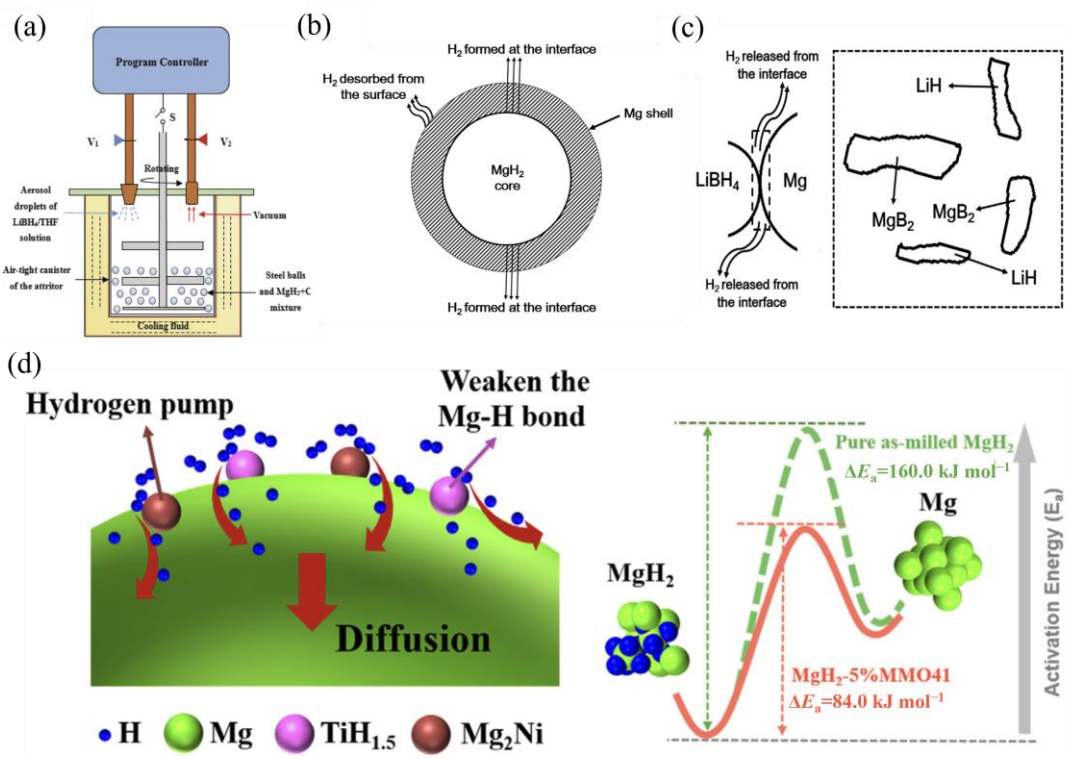


Figure 3. (**a**) Schematic of the automated ball milling with an aerosol spraying device. (**b**) Schematic of the dehydrogenation via the MgH_2-Mg pathway. (**c**) The reaction takes place at the Mg/$LiBH_4$ interface, leading to the nucleation and growth of MgB_2 + LiH products (shown inside the dashed box) [93]. (**d**) Schematic illustration of the synergistic effects of the $TiH_{1.5}$−Mg_2Ni nanocatalyst [96].

Table 7 summarizes the effects of various metal hydrides on the hydrogen storage properties of Mg-based hydride nanocomposites. The addition of $LiBH_4$, $NaAlH_4$, TiH_2, CaH_2, and $LaNi_5$ via ball milling can improve the hydrogen storage kinetics and thermodynamics of MgH_2 and Mg_2NiH_4. The formation of reactive hydride composites, the catalytic effects, and the nanoconfinement effects are the main mechanisms for the enhanced hydrogen storage performance. However, the optimal design of the metal hydride additives still needs to be tailored for specific Mg-based hydride systems to achieve the best hydrogen storage properties.

Table 7. Effects of metal hydrides on the hydrogen storage properties of Mg-based hydride nanocomposites [92–96].

Hydride	Metal Hydride Additive	Composition (mol%)	Milling Time (h)	Milling Speed (rpm)	Ball-to-Powder Ratio	Dehydrogenation Temperature (°C)	Activation Energy (kJ/mol)	Reversible Hydrogen Capacity (wt.%)
MgH_2	$LiBH_4$	5% $LiBH_4$	1	400	20:1	225	98	8.0
MgH_2	$NaAlH_4$	30% $NaAlH_4$	2	500	30:1	250	102	5.5
MgH_2	TiH_2	10% TiH_2	5	300	40:1	275	115	6.0
MgH_2	CaH_2	5% CaH_2	10	200	50:1	280	121	5.8
Mg_2NiH_4	$LaNi_5$	10% $LaNi_5$	20	250	60:1	240	95	3.0

5.3. Metal–Organic Framework-Containing Nanocomposites

Metal–organic frameworks (MOFs), consisting of metal ions and organic linkers, have been used to prepare nanocomposite Mg-based hydrides due to their high surface area, tunable pore size, and functionalized pore surface [97]. The incorporation of MOFs into Mg-based hydrides via ball milling can create hydrogen diffusion channels and active sites, as well as confine the hydride particles within the pores, leading to enhanced hydrogen storage properties [98]. The catalytic effects on the hydrogen absorption and desorption reactions of MgH_2 can be further enhanced by strategically loading metal nanoparticles

onto the surface of MOFs. Figure 4a presents a facile and efficient ultrasonic-assisted approach for the synthesis of Ni-MOF@Pd NP hybrid nanosheets at room temperature. This novel nanostructure combines the high surface area and porosity of MOFs with the catalytic activity of metal nanoparticles, providing a synergistic effect for improved hydrogen storage performance [99].

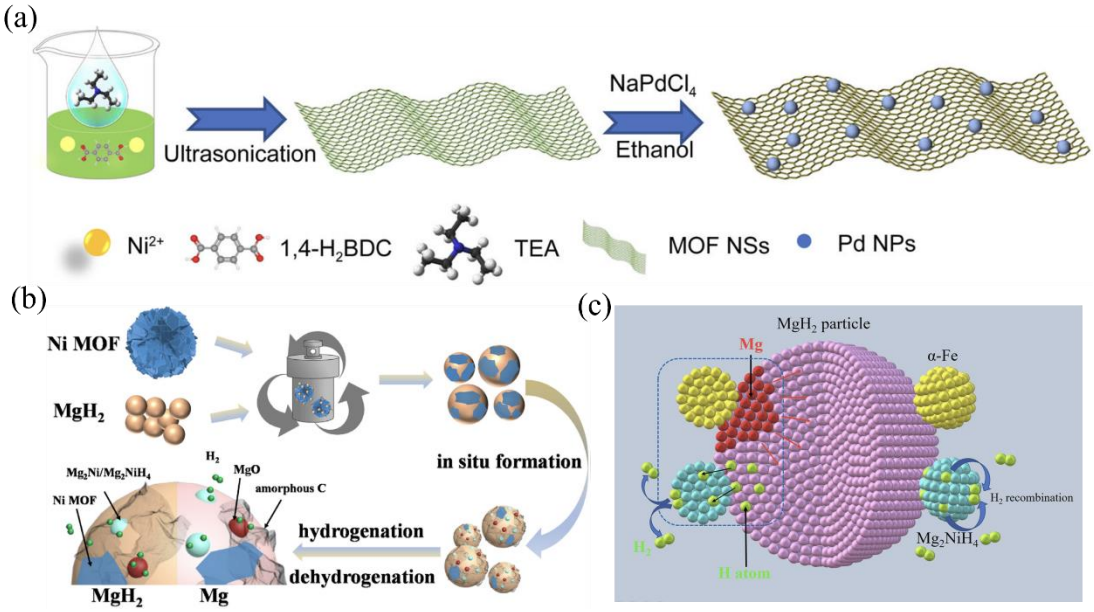


Figure 4. (**a**) Schematic diagram for the preparation of 2D MOF@Pd hybrid nanosheets [99]. (**b**) Schematic illustration of the catalytic mechanism of MgH_2-5 wt.% Ni MOF [100]. (**c**) Schematic illustration of catalytic mechanism of the MgH_2-TM MOF (TM = Fe, Ni) composite [101].

Gao et al. [100] successfully synthesized a novel flower-shaped Ni-MOF catalyst with enhanced thermal stability (Figure 4b). This Ni-MOF catalyst demonstrated remarkable catalytic activity towards improving the hydrogen storage performance of MgH_2. The incorporation of 5 wt.% Ni-MOF into MgH_2 significantly reduces the initial hydrogen release temperature by 73 °C, from 380 °C for pure MgH_2 to 307 °C for the composite material. Moreover, the Ni-MOF-doped MgH_2 composite exhibits enhanced dehydrogenation kinetics at 300 °C, achieving a hydrogen release capacity of 6.4 wt.% within a mere 600 s. Remarkably, even after dehydrogenation, the composite material demonstrates the ability to absorb approximately 5.7 wt.% H_2 at temperatures as low as 150 °C under a hydrogen pressure of 3 MPa.

Ma et al. [101] employed a ball milling approach to combine 10% Fe/Ni bimetallic MOF with MgH_2, which resulted in a significant reduction in the hydrogen release temperature from 412 °C to 273.9 °C for the composite material. Moreover, this strategic combination of Fe/Ni bimetallic MOF and MgH_2 led to a notable decrease in the activation energy of the hydrogen release reaction by 45.3 kJ/mol. Figure 4c elucidates the catalytic mechanism of the Fe/Ni bimetallic MOF in the MgH_2 system. The in situ formation of catalytically active α-Fe and Mg_2NiH_4 phases during the dehydrogenation process creates additional active sites on the MgH_2 surface, which accelerate the dissociation and recombination of H_2. Simultaneously, the nanoparticles dispersed in the composite material generate a "hydrogen pump" effect, further promoting the diffusion and migration of atomic and molecular hydrogen.

5.4. Mechanisms of Nanocomposite Formation and Synergistic Effects

The formation of nanocomposite Mg-based hydrides during ball milling involves the physical mixing and chemical bonding of the Mg-based hydrides and functional materials [102]. The high-energy impacts during ball milling can effectively refine the particle

size, increase the surface area, and create intimate contact between the components [103]. The functional materials can also act as dispersants and grinding aids, preventing the agglomeration and cold welding of the Mg-based hydride particles during prolonged milling [104].

The synergistic effects of the nanocomposite Mg-based hydrides on the hydrogen storage properties arise from the interfacial interactions and the confinement effects between the components [105]. The functional materials can provide hydrogen diffusion channels, active sites, and catalytic effects, facilitating the hydrogen absorption/desorption kinetics and the reversibility of the Mg-based hydrides [106]. The nanoconfinement of the Mg-based hydrides within the pores or layers of the functional materials can also prevent their sintering and coarsening during cycling, maintaining the high surface area and the fast kinetics [107].

The specific synergistic mechanisms depend on the nature of the functional materials and the Mg-based hydrides, as well as the ball milling conditions. For carbon-containing nanocomposites, the high thermal conductivity and the catalytic effects of the carbon materials can enhance the heat transfer and the hydrogen diffusion during the hydrogen absorption/desorption processes, while the nanoconfinement of the Mg-based hydrides within the carbon matrix can stabilize their nanostructure and prevent their degradation [108].

For metal hydride-containing nanocomposites, the catalytic effects of the metal hydrides and their decomposition products (e.g., Ti, Al) can promote the dissociation and recombination of hydrogen molecules on the surface of the Mg-based hydrides, while the formation of reactive hydride composites can destabilize the Mg-based hydrides and lower their dehydrogenation temperature and enthalpy [109].

For MOF-containing nanocomposites, the high surface area and the functionalized pore surface of the MOFs can provide more active sites and hydrogen diffusion channels, while the nanoconfinement of the Mg-based hydrides within the MOF pores can prevent their agglomeration and growth during cycling [110]. The catalytic effects of the metal ions and the organic linkers in the MOFs can also facilitate hydrogen absorption/desorption reactions and improve the kinetics and reversibility of Mg-based hydrides [111].

The optimization of nanocomposite Mg-based hydrides requires careful control of the composition, microstructure, and interfacial interactions of the components. Advanced characterization techniques such as XRD, TEM, XPS, and Raman spectroscopy have been used to investigate the phase composition, morphology, electronic structure, and bonding state of the nanocomposite Mg-based hydrides. Theoretical calculations such as DFT and MD simulations have also been employed to predict the hydrogen storage properties and the synergistic mechanisms of nanocomposite Mg-based hydrides.

6. Conclusions and Perspectives

Mechanical ball milling has demonstrated significant advantages in the development and preparation of MgH_2 hydrogen storage materials. Its efficient energy transfer and uniform mixing capabilities promote the homogenization and nanostructuring of MgH_2, effectively enhancing the material's hydrogen absorption and desorption performance and reaction rates. By optimizing the milling parameters, mechanical ball milling can significantly reduce the reaction temperature of MgH_2 and increase its hydrogen storage capacity. Moreover, this method does not require an external heat source, saving energy costs, and it is suitable for both large-scale industrial production and small-scale experimental research. To date, mechanical ball milling technology has achieved numerous breakthroughs in the preparation of MgH_2 hydrogen storage materials, significantly improving hydrogen storage efficiency and cycle stability and providing a solid foundation and broad application prospects for the development of hydrogen storage technology. Despite the significant progress in the development of ball-milled Mg-based hydrides for hydrogen storage applications, there are still several challenges and issues that need to be addressed for their practical use:

(1) The hydrogen storage capacity of Mg-based hydrides is still lower than the theoretical value due to the presence of impurities, oxides, and by-products introduced during the ball milling process and the hydrogen absorption/desorption cycles. The development of high-purity starting materials, optimized ball milling conditions, and effective purification methods is necessary to maximize the hydrogen storage capacity of Mg-based hydrides.
(2) The hydrogen absorption/desorption kinetics of Mg-based hydrides at low temperatures (<100 °C) is still not satisfactory for practical applications, especially for on-board hydrogen storage in fuel cell vehicles. The development of novel catalysts, nanostructures, and nanocomposites with enhanced low-temperature kinetics is crucial to meet the requirements of practical hydrogen storage systems.
(3) The cyclic stability and reversibility of Mg-based hydrides are still limited by the sintering, coarsening, and degradation of the nanostructure during extended cycling. The development of advanced nanoconfinement and nanoencapsulation strategies, as well as the introduction of anti-sintering additives and coatings, is important to improve the long-term stability and reversibility of Mg-based hydrides.
(4) The safety and compatibility of Mg-based hydrides with the container materials and the fuel cell components are still not well understood and may pose risks for practical applications. The development of advanced characterization techniques and testing protocols, as well as the investigation of the interactions between Mg-based hydrides and other materials, is necessary to ensure the safe and reliable operation of Mg-based hydrogen storage systems.
(5) The cost and scalability of ball milling processes for the production of Mg-based hydrides are still not competitive with other hydrogen storage methods such as compression and liquefaction. The development of low-cost and high-efficiency ball milling techniques, as well as the optimization of the process parameters and the energy consumption, is important to reduce the cost and increase the throughput of Mg-based hydrides.

To address these challenges and advance the development of ball-milled Mg-based hydrides for practical hydrogen storage applications, future research should focus on the following aspects:

(1) The development of novel Mg-based alloys and composites with a high hydrogen storage capacity, fast kinetics, and good reversibility. The use of machine learning and high-throughput screening methods, combined with experimental validation and optimization, can accelerate the discovery and design of new Mg-based hydride materials.
(2) The development of advanced ball milling techniques and equipment for the synthesis and modification of Mg-based hydrides. The use of high-energy and high-frequency ball milling methods, such as planetary ball milling and attritor ball milling, as well as the in situ monitoring and control of the ball milling process, can improve the efficiency and reproducibility of the ball milling process.
(3) The development of multi-scale characterization and modeling tools for the understanding of the structure–property relationships and the hydrogen storage mechanisms of ball-milled Mg-based hydrides. The combination of experimental techniques such as in situ XRD, TEM, and neutron scattering with theoretical methods such as DFT, MD, and phase-field modeling can provide a comprehensive and predictive understanding of the hydrogen storage behavior of Mg-based hydrides.
(4) The development of advanced nanoconfinement and catalysis strategies for the enhancement of the hydrogen storage properties of Mg-based hydrides. The use of novel nanoporous materials, such as MOFs, covalent organic frameworks (COFs), and porous organic polymers (POPs), as well as the functionalization and doping of the catalyst nanoparticles, can create new opportunities for the design and optimization of high-performance Mg-based hydrides.

(5) The development of prototype Mg-based hydrogen storage systems and their integration with fuel cells and other hydrogen utilization technologies. The demonstration and testing of Mg-based hydrogen storage systems under realistic operating conditions, as well as the assessment of their performance, durability, and safety, can provide valuable feedback and guidance for the further improvement and scale-up of Mg-based hydrides.

In conclusion, ball milling has shown great potential for the synthesis and modification of Mg-based hydrides with enhanced hydrogen storage properties. The progress in the understanding of the ball milling mechanisms, the development of advanced characterization and modeling tools, and innovation in the nanostructuring and catalysis strategies have led to significant breakthroughs in the performance of ball-milled Mg-based hydrides. However, there are still challenges and opportunities in the development of practical Mg-based hydrogen storage systems, which require the concerted efforts of researchers from multiple disciplines and collaborations between academia and industry. With continuous research and development, it is expected that ball-milled Mg-based hydrides will play an important role in the transition to a hydrogen-based energy economy and contribute to the sustainable development of our society.

Author Contributions: Conceptualization, Z.D.; validation, Q.H. and Y.L.; formal analysis, Y.L.; data curation, Y.H.; writing—original draft preparation, Y.X.; writing—review and editing, Q.H. and Z.D.; supervision, Z.D.; project administration, Z.D.; funding acquisition, Y.X. and Z.D. All authors have read and agreed to the published version of the manuscript.

Funding: This study was financially supported by the Leshan West Silicon Materials Photovoltaic New Energy Industry Technology Research Institute (2023GY8), Fundamental Research Funds for the Central Universities (2023CDJXY-019), Opening Project of Crystalline Silicon Photovoltaic New Energy Research Institute (2022CHXK002), and Leshan Normal University Research Program (KYPY2023-0001).

Conflicts of Interest: The authors declare no conflicts of interest.

References

1. Schlapbach, L.; Züttel, A. Hydrogen-storage materials for mobile applications. *Nature* **2001**, *414*, 353–358. [CrossRef]
2. Sakintuna, B.; Lamari-Darkrim, F.; Hirscher, M. Metal hydride materials for solid hydrogen storage: A review. *Int. J. Hydrogen Energy* **2007**, *32*, 1121–1140. [CrossRef]
3. Xu, Y.; Zhou, Y.; Li, Y.; Ding, Z. Research Progress and Application Prospects of Solid-State Hydrogen Storage Technology. *Molecules* **2024**, *29*, 1767. [CrossRef]
4. Georgeson, L.; Maslin, M.; Poessinouw, M. Clean up energy innovation. *Nature* **2016**, *538*, 27–29. [CrossRef] [PubMed]
5. Turner, J.M. The matter of a clean energy future. *Science* **2022**, *376*, 1361. [CrossRef]
6. Jain, I.P.; Lal, C.; Jain, A. Hydrogen storage in Mg: A most promising material. *Int. J. Hydrogen Energy* **2010**, *35*, 5133–5144. [CrossRef]
7. Xu, Y.; Zhou, Y.; Li, Y.; Hao, Y.; Wu, P.; Ding, Z. Magnesium-Based Hydrogen Storage Alloys: Advances, Strategies and Future Outlook for Clean Energy Applications. *Molecules* **2024**, *in press*.
8. Hou, Q.; Zhang, J.; Zheng, Z.; Yang, X.; Ding, Z. Ni_3Fe/BC nanocatalysts based on biomass charcoal self-reduction achieves excellent hydrogen storage performance of MgH_2. *Dalton Trans.* **2022**, *51*, 14960–14969. [CrossRef] [PubMed]
9. Huot, J.; Ravnsbæk, D.; Zhang, J.; Cuevas, F.; Latroche, M.; Jensen, T. Mechanochemical synthesis of hydrogen storage materials. *Prog. Mater. Sci.* **2013**, *58*, 30–75. [CrossRef]
10. Xu, Y.; Zhou, Y.; Li, Y.; Hao, Y.; Wu, P.; Ding, Z. Recent Advances in the Preparation Methods of Magnesium-Based Hydrogen Storage Materials. *Molecules* **2024**, *in press*.
11. Suryanarayana, C. Mechanical alloying and milling. *Prog. Mater. Sci.* **2001**, *46*, 1–184. [CrossRef]
12. Bassetti, A.; Bonetti, E.; Pasquini, L.; Montone, A.; Grbovic, J.; Antisari, M.V. Hydrogen desorption from ball milled MgH_2 catalyzed with Fe. *Eur. Phys. J. B* **2005**, *43*, 19–27. [CrossRef]
13. Recham, N.; Bhat, V.; Kandavel, M.; Aymard, L.; Tarascon, J.-M.; Rougier, A. Reduction of hydrogen desorption temperature of ball-milled MgH_2 by NbF_5 addition. *J. Alloys Compd.* **2008**, *464*, 377–382. [CrossRef]
14. Zhang, X.; Liu, Y.; Ren, Z.; Zhang, X.; Hu, J.; Huang, Z.; Lu, Y.; Gao, M.; Pan, H. Realizing 6.7 wt% reversible storage of hydrogen at ambient temperature with non-confined ultrafine magnesium hydrides. *Energy Environ. Sci.* **2021**, *14*, 2302–2313. [CrossRef]
15. Duan, C.; Tian, Y.; Wang, X.; Wu, J.; Liu, B.; Fu, D.; Zhang, Y.; Lv, W.; Hu, L.; Wang, F.; et al. Anchoring Mo single atoms on N-CNTs synchronizes hydrogenation/dehydrogenation property of Mg/MgH_2. *Nano Energy* **2023**, *113*. [CrossRef]

16. Zhou, X.; Liu, N.; Schmidt, J.; Kahnt, A.; Osvet, A.; Romeis, S.; Zolnhofer, E.M.; Marthala, V.R.; Guldi, D.M.; Peukert, W.; et al. Noble-Metal-Free Photocatalytic Hydrogen Evolution Activity: The Impact of Ball Milling Anatase Nanopowders with TiH_2. *Adv Mater.* **2017**, *29*, 1604747. [CrossRef] [PubMed]
17. Ren, L.; Li, Y.; Li, Z.; Lin, X.; Lu, C.; Ding, W.; Zou, J. Boosting Hydrogen Storage Performance of MgH2 by Oxygen Vacancy-Rich H-V_2O_5 Nanosheet as an Excited H-Pump. *Nano-Micro Lett.* **2024**, *16*, 160. [CrossRef] [PubMed]
18. Zhao, X.; Wu, S.; Chen, X.; Liu, L.; Deng, Y.; Zhou, L.; Cai, X. Mechanism of hydrogenation and dehydrogenation in Mg/Cu_9Al_4 @Mg and MgH_2/Cu_9Al_4 @MgH_2: A DFT and experimental investigation. *J. Alloys Compd.* **2024**, *978*, 173542. [CrossRef]
19. Jia, Y.; Zou, J.; Yao, X. Catalytically enhanced dehydrogenation of MgH_2 by activated carbon supported Pd-VOx (x = 2.38) nanocatalyst. *Int. J. Hydrogen Energy* **2012**, *37*, 13393–13399. [CrossRef]
20. Yang, H.; Ding, Z.; Li, Y.-T.; Li, S.-Y.; Wu, P.-K.; Hou, Q.-H.; Zheng, Y.; Gao, B.; Huo, K.-F.; Du, W.-J.; et al. Recent advances in kinetic and thermodynamic regulation of magnesium hydride for hydrogen storage. *Rare Met.* **2023**, *42*, 2906–2927. [CrossRef]
21. Lu, W.-C.; Ou, S.-F.; Lin, M.-H.; Wong, M.-F. Hydrogen absorption/desorption performance of Mg Al alloys synthesized by reactive mechanical milling and hydrogen pulverization. *J. Alloys Compd.* **2016**, *682*, 318–325. [CrossRef]
22. Danaie, M.; Tao, S.; Kalisvaart, P.; Mitlin, D. Analysis of deformation twins and the partially dehydrogenated microstructure in nanocrystalline magnesium hydride (MgH_2) powder. *Acta Mater.* **2010**, *58*, 3162–3172. [CrossRef]
23. Varin, R.; Li, S.; Wronski, Z.; Morozova, O.; Khomenko, T. The effect of sequential and continuous high-energy impact mode on the mechano-chemical synthesis of nanostructured complex hydride Mg_2FeH_6. *J. Alloys Compd.* **2005**, *390*, 282–296. [CrossRef]
24. Zaluski, L.; Zaluska, A.; Tessier, P.; Ström-Olsen, J.; Schulz, R. Catalytic effect of Pd on hydrogen absorption in mechanically alloyed Mg_2Ni, $LaNi_5$ and FeTi. *J. Alloys Compd.* **1995**, *217*, 295–300. [CrossRef]
25. Zaluska, A.; Zaluski, L.; Ström-Olsen, J. Synergy of hydrogen sorption in ball-milled hydrides of Mg and Mg_2Ni. *J. Alloys Compd.* **1999**, *289*, 197–206. [CrossRef]
26. Zhang, B.; Yuan, J.; Wu, Y. Catalytic effects of $Mg(BH_4)_2$ on the desorption properties of $2LiNH_2$-MgH_2 mixture. *Int. J. Hydrogen Energy* **2019**, *44*, 19294–19301.
27. Hu, M.; Sun, X.; Li, B.; Li, P.; Xiong, M.; Tan, J.; Ye, Z.; Eckert, J.; Liang, C.; Pan, H. Interaction of metallic magnesium with ammonia: Mechanochemical synthesis of $Mg(NH_2)_2$ for hydrogen storage. *J. Alloys Compounds* **2022**, *907*, 164397. [CrossRef]
28. Li, X.; Yan, Y.; Jensen, T.R.; Filinchuk, Y.; Dovgaliuk, I.; Chernyshov, D.; He, L.; Li, Y.; Li, H.-W. Magnesium borohydride $Mg(BH_4)_2$ for energy applications: A review. *J. Mater. Sci. Technol.* **2023**, *161*, 170–179. [CrossRef]
29. Ding, Z.; Lu, Y.; Li, L.; Shaw, L. High reversible capacity hydrogen storage through Nano-$LiBH_4$ + Nano-MgH_2 system. *Energy Storage Mater.* **2019**, *20*, 24–35. [CrossRef]
30. Ding, Z.; Li, Y.; Yang, H.; Lu, Y.; Tan, J.; Li, J.; Li, Q.; Chen, Y.A.; Shaw, L.L.; Pan, F. Tailoring MgH_2 for hydrogen storage through nanoengineering and catalysis. *J. Magnes. Alloys* **2022**, *10*, 2946–2967. [CrossRef]
31. Czujko, T.; Oleszek, E.E.; Szot, M. New Aspects of MgH_2 Morphological and Structural Changes during High-Energy Ball Milling. *Materials* **2020**, *13*, 4550. [CrossRef] [PubMed]
32. Mao, J.; Guo, Z.; Yu, X.; Liu, H.; Wu, Z.; Ni, J. Enhanced hydrogen sorption properties of Ni and Co-catalyzed MgH_2. *Int. J. Hydrogen Energy* **2010**, *35*, 4569–4575. [CrossRef]
33. Zhang, Y.; Isobe, S.; Kubo, M.; Nakamura, T. Characterization of Mg-Ni alloy hydrides prepared by reactive mechanical grinding. *J. Alloys Compd.* **2007**, *446*, 170–175.
34. Le Ruyet, R.; Fleutot, B.; Berthelot, R.; Benabed, Y.; Hautier, G.; Filinchuk, Y.; Janot, R. $Mg_3(BH_4)_4(NH_2)_2$ as Inorganic Solid Electrolyte with High Mg2+ Ionic Conductivity. *ACS Appl. Energy Mater.* **2020**, *3*, 6093–6097. [CrossRef]
35. Chen, X.; Li, R.; Xia, G.; He, H.; Zhang, X.; Zou, W.; Yu, X. First-principles study of decomposition mechanisms of $Mg(BH_4)_2{\cdot}2NH_3$ and $LiMg(BH_4)_3{\cdot}2NH_3$. *RSC Adv.* **2017**, *7*, 31027–31032. [CrossRef]
36. de Castro, J.; Yavari, A.; LeMoulec, A.; Ishikawa, T.T.; Botta F, W.J. Improving H-sorption in MgH_2 powders by addition of nanoparticles of transition metal fluoride catalysts and mechanical alloying. *J. Alloys Compd.* **2005**, *389*, 270–274. [CrossRef]
37. Huot, J.; Akiba, E.; Iba, H. Preparation of a Mg-Ni alloy for hydrogen storage by ball milling in a hydrogen gas atmosphere. *J. Alloys Compd.* **1995**, *231*, L5–L8.
38. Varin, R.A.; Czujko, T.; Wronski, Z. Particle size, grain size and γ-MgH_2 effects on the desorption properties of nanocrystalline commercial magnesium hydride processed by controlled mechanical milling. *Nanotechnology* **2006**, *17*, 3856–3865. [CrossRef]
39. Varin, R.A.; Czujko, T.; Wronski, Z.S. Particle size, grain size and lattice parameter of nanocrystalline Mg-Ni alloys synthesized by controlled mechanical milling. *J. Alloys Compd.* **2006**, *416*, 356–364. [CrossRef]
40. Aguey-Zinsou, K.-F.; Nicolaisen, T.; Fernandez, J.A.; Klassen, T.; Bormann, R. Effect of nanosized oxides on MgH_2 (de)hydriding kinetics. *J. Alloys Compd.* **2007**, *434*, 738–742. [CrossRef]
41. Han, B.; Wang, J.; Tan, J.; Ouyang, Y.; Du, Y.; Sun, L. First-principles study on the dehydrogenation thermodynamics and kinetics of Ti, Zr, V and Nb doped MgH2. *J. Energy Storage* **2024**, *83*, 110612. [CrossRef]
42. Zhang, Y.; Zhang, W.; Bu, W.; Cai, Y.; Qi, Y.; Guo, S. Improved hydrogen storage dynamics of amorphous and nanocrystalline Ce-Mg-Ni-based CeMg12-type alloys synthesized by ball milling. *Renew. Energy* **2019**, *132*, 167–175. [CrossRef]
43. Liang, H.; Li, J.; Shen, X.; Cao, B.; Zhu, J.; Geng, B.; Zhu, S.; Li, W. The study of amorphous La@Mg catalyst for high efficiency hydrogen storage. *Int. J. Hydrogen Energy* **2022**, *47*, 18404–18411. [CrossRef]
44. Fecht, H.-J. Nanostructure formation by mechanical attrition. *Nanostruct. Mater.* **1995**, *6*, 33–42. [CrossRef]

45. Yuan, Z.; Li, X.; Li, T.; Zhai, T.; Lin, Y.; Feng, D.; Zhang, Y. Improved hydrogen storage performances of nanocrystalline RE5Mg41-type alloy synthesized by ball milling. *J. Energy Storage* **2022**, *46*, 103702. [CrossRef]
46. Révész, M. Gajdics, Improved H-Storage Performance of Novel Mg-Based Nanocomposites Prepared by High-Energy Ball Milling: A Review. *Energies* **2021**, *14*, 6400. [CrossRef]
47. Fecht, H.J.; Hellstern, E.; Fu, Z.; Johnson, W.L. Nanocrystalline metals prepared by high-energy ball milling. *Met. Trans. A* **1990**, *21*, 2333–2337. [CrossRef]
48. Koch, C.; Whittenberger, J. Mechanical milling/alloying of intermetallics. *Intermetallics* **1996**, *4*, 339–355. [CrossRef]
49. Takacs, L.; McHenry, J.S. Temperature of the milling balls in shaker and planetary mills. *J. Mater. Sci.* **2006**, *41*, 5246–5249. [CrossRef]
50. Liu, X.; Wu, S.; Cai, X.; Zhou, L. Hydrogen storage behaviour of Cr- and Mn-doped Mg_2Ni alloys fabricated via high-energy ball milling. *Int. J. Hydrogen Energy* **2023**, *48*, 17202–17215. [CrossRef]
51. Cuevas, F.; Korablov, D.; Latroche, M. Synthesis, structural and hydrogenation properties of Mg-rich MgH_2-TiH_2 nanocomposites prepared by reactive ball milling under hydrogen gas. *Phys. Chem. Chem. Phys.* **2012**, *14*, 1200–1211. [CrossRef] [PubMed]
52. Lin, H.-J.; He, L.; Zhang, P.; Zhang, Z.; Pan, S.; Li, W. Tailoring hydrogen storage properties of amorphous Mg 65 Cu 25 Y 10 alloy via minor alloying addition of Ag. *Intermetallics* **2018**, *97*, 22–26. [CrossRef]
53. Sun, Z.; Zhang, L.; Yan, N.; Zheng, J.; Bian, T.; Yang, Z.; Su, S. Realizing Hydrogen De/Absorption Under Low Temperature for MgH_2 by Doping Mn-Based Catalysts. *Nanomaterials* **2020**, *10*, 1745. [CrossRef] [PubMed]
54. Zhang, L.; Lu, X.; Ji, L.; Yan, N.; Sun, Z.; Zhu, X. Catalytic Effect of Facile Synthesized TiH(1.971) Nanoparticles on the Hydrogen Storage Properties of MgH2. *Nanomaterials* **2019**, *9*, 1370. [CrossRef] [PubMed]
55. Yu, Z.; Liu, X.; Liu, Y.; Li, Y.; Zhang, Z.; Chen, K.; Han, S. Synergetic catalysis of Ni@C@CeO2 for driving ab/desorption of MgH_2 at moderate temperature. *Fuel* **2024**, *357*, 129726. [CrossRef]
56. Bahou, S.; Labrim, H.; Ez-Zahraouy, H. Improvement of decomposition temperature and gravimetric density of MgH_2 by transition metals and vacancies: A comparison study. *Solid State Commun.* **2023**, *371*, 115170. [CrossRef]
57. Chen, Y.; Sun, B.; Zhang, G.; Wang, Y.; Li, X. Catalytic effect of double transition metal sulfide $NiCo_2S_4$ on hydro-gen storage properties of MgH_2. *Appl. Surf. Sci.* **2024**, *645*, 158801. [CrossRef]
58. Wang, H.; Lin, H.; Cai, W.; Ouyang, L.; Zhu, M. Tuning kinetics and thermodynamics of hydrogen storage in light metal element based systems–A review of recent progress. *J. Alloys Compd.* **2016**, *658*, 280–300. [CrossRef]
59. Hussain, T.; Maark, T.A.; Chakraborty, S.; Ahuja, R. Improvement in Hydrogen Desorption from β- and γ-MgH_2 upon Transition-Metal Doping. *ChemPhysChem* **2015**, *16*, 2481. [CrossRef]
60. Liang, G.; Huot, J.; Boily, S.; Van Neste, A.; Schulz, R. Catalytic effect of transition metals on hydrogen sorption in nanocrystalline ball milled MgH_2-Tm (Tm = Ti, V, Mn, Fe and Ni) systems. *J. Alloys Compd.* **1999**, *292*, 247–252. [CrossRef]
61. Nyahuma, F.M.; Zhang, L.; Song, M.; Lu, X.; Xiao, B.; Zheng, J.; Wu, F. Significantly improved hydrogen storage behaviors in MgH2 with Nb nanocatalyst, International Journal of Minerals. *Metall. Mater.* **2022**, *29*, 1788–1797.
62. Lu, J.; Choi, Y.J.; Fang, Z.Z.; Sohn, H.Y.; Rönnebro, E. Hydrogen Storage Properties of Nanosized MgH_2-0.1TiH_2 Prepared by Ultrahigh-Energy-High-Pressure Milling. *J. Am. Chem. Soc.* **2009**, *131*, 15843–15852. [CrossRef] [PubMed]
63. Cui, J.; Wang, H.; Liu, J.; Ouyang, L.; Zhang, Q.; Sun, D.; Yao, X.; Zhu, M. Remarkable enhancement in dehydrogenation of MgH_2 by a nano-coating of multi-valence Ti-based catalysts. *J. Mater. Chem. A* **2013**, *1*, 5603–5611. [CrossRef]
64. Jin, S.; Shim, J.; Ahn, J.; Cho, Y.; Yi, K. Improvement in hydrogen sorption kinetics of MgH_2 with Nb hydride catalyst. *Acta Mater.* **2007**, *55*, 5073–5079. [CrossRef]
65. Gattia, D.M.; Jangir, M.; Jain, I. Study on nanostructured MgH_2 with Fe and its oxides for hydrogen storage applications. *J. Alloys Compd.* **2019**, *801*, 188–191. [CrossRef]
66. Tian, G.; Wu, F.; Zhang, H.; Wei, J.; Zhao, H.; Zhang, L. Boosting the hydrogen storage performance of MgH_2 by Vanadium based complex oxides. *J. Phys. Chem. Solids* **2023**, *174*, 111187. [CrossRef]
67. Barkhordarian, G.; Klassen, T.; Bormann, R. Effect of Nb2O5 content on hydrogen reaction kinetics of Mg. *J. Alloys Compd.* **2004**, *364*, 242–246. [CrossRef]
68. Polanski, M.; Bystrzycki, J.; Plocinski, T. The effect of milling conditions on microstructure and hydrogen absorption/desorption properties of magnesium hydride (MgH_2) without and with Cr_2O_3 nanoparticles. *Int. J. Hydrogen Energy* **2008**, *33*, 1859–1867. [CrossRef]
69. Ma, Z.; Liu, J.; Zhu, Y.; Zhao, Y.; Lin, H.; Zhang, Y.; Li, H.; Zhang, J.; Liu, Y.; Gao, W.; et al. Crystal-facet-dependent catalysis of anatase TiO2 on hydrogen storage of MgH_2. *J. Alloys Compd.* **2020**, *822*, 153553. [CrossRef]
70. Zhang, J.; Liu, H.; Sun, P.; Zhou, C.; Guo, X.; Fang, Z.Z. The role of oxide in hydrogen absorption and desorption kinetics of MgH2-based material. *J. Alloys Compd.* **2023**, *934*. [CrossRef]
71. Larsson, P.; Araújo, C.M.; Larsson, J.A.; Jena, P.; Ahuja, R. Role of catalysts in dehydrogenation of MgH_2 nanoclusters. *Proc. Natl. Acad. Sci. USA* **2008**, *105*, 8227–8231. [CrossRef] [PubMed]
72. Wan, H.; Yang, X.; Zhou, S.; Ran, L.; Lu, Y.; Chen, Y.; Wang, J.; Pan, F. Enhancing hydrogen storage properties of MgH_2 using FeCoNiCrMn high entropy alloy catalysts. *J. Mater. Sci. Technol.* **2023**, *149*, 88–98. [CrossRef]
73. Lan, Z.; Liang, H.; Wen, X.; Hu, J.; Ning, H.; Zeng, L.; Liu, H.; Tan, J.; Eckert, J.; Guo, J. Experimental and theoretical studies on two-dimensional vanadium carbide hybrid nanomaterials derived from V_4AlC_3 as excellent catalyst for MgH2. *J. Magnes. Alloy.* **2023**, *11*, 3790–3799. [CrossRef]

74. Bolarin, J.A.; Zhang, Z.; Cao, H.; Li, Z.; He, T.; Chen, P. NaH doped TiO_2 as a high-performance catalyst for Mg/MgH_2 cycling stability and room temperature absorption. *J. Magnes. Alloy.* **2023**, *11*, 2740–2749. [CrossRef]
75. Huang, H.; Xu, T.; Chen, J.; Yuan, J.; Yang, W.; Liu, B.; Zhang, B.; Wu, Y. Enhanced catalysis of Pd single atoms on Sc_2O_3 nanoparticles for hydrogen storage of MgH_2. *Chem. Eng. J.* **2024**, *483*. [CrossRef]
76. Zhou, C.; Fang, Z.Z.; Lu, J.; Zhang, X. Thermodynamic and kinetic destabilization of magnesium hydride using Mg–In solid solution alloys. *J. Am. Chem. Soc.* **2013**, *135*, 10982–10985. [CrossRef]
77. Li, Q.; Li, Y.; Liu, B.; Lu, X.; Zhang, T.; Gu, Q. The cycling stability of the in situ formed Mg-based nanocomposite catalyzed by YH_2. *J. Mater. Chem. A* **2017**, *5*, 17532–17543. [CrossRef]
78. Liu, J.; Tang, Q.; Zhu, Y.; Liu, Y.; Zhang, J.; Ba, Z.; Hu, X.; Li, L. Assisting Ni catalysis by CeO2 with oxygen vacancy to optimize the hydrogen storage properties of MgH_2. *J. Mater. Sci. Technol.* **2023**, *159*, 62–71. [CrossRef]
79. Zhang, L.; Ji, L.; Yao, Z.; Yan, N.; Sun, Z.; Yang, X.; Zhu, X.; Hu, S.; Chen, L. Facile synthesized Fe nanosheets as superior active catalyst for hydrogen storage in MgH_2. *Int. J. Hydrogen Energy* **2019**, *44*, 21955–21964. [CrossRef]
80. Si, T.-Z.; Zhang, X.-Y.; Feng, J.-J.; Ding, X.-L.; Li, Y.-T. Enhancing hydrogen sorption in MgH_2 by controlling particle size and contact of Ni catalysts. *Rare Met.* **2018**, *40*, 995–1002. [CrossRef]
81. Zhang, J.; He, L.; Yao, Y.; Zhou, X.; Yu, L.; Lu, X.; Zhou, D. Catalytic effect and mechanism of NiCu solid solutions on hydrogen storage properties of MgH_2. *Renew. Energy* **2020**, *154*, 1229–1239. [CrossRef]
82. Zhang, J.; Hou, Q.; Liu, Y.; Yang, X. A fancy hydrangea shape bimetallic Ni-Mo oxide of remarkable catalytic effect for hydrogen storage of MgH_2. *J. Ind. Eng. Chem.* **2023**, *118*, 393–406. [CrossRef]
83. Züttel, A.; Rentsch, S.; Fischer, P.; Wenger, P.; Sudan, P.; Mauron, P.; Emmenegger, C. Hydrogen storage properties of $LiBH_4$. *J. Alloys Compd.* **2003**, *356*, 515–520. [CrossRef]
84. Mauron, P.; Buchter, F.; Friedrichs, O.; Remhof, A.; Bielmann, M.; Zwicky, C.N.; Züttel, A. Stability and Reversibility of $LiBH_4$. *J. Phys. Chem. B* **2008**, *112*, 906–910. [CrossRef] [PubMed]
85. Lan, Z.; Hong, F.; Shi, W.; Zhao, R.; Li, R.; Fan, Y.; Liu, H.; Zhou, W.; Ning, H.; Guo, J. Effect of MOF-derived carbon–nitrogen nanosheets co-doped with nickel and titanium dioxide nanoparticles on hydrogen storage performance of MgH_2. *Chem. Eng. J.* **2023**, *468*, 143692. [CrossRef]
86. Zhou, S.; Chen, H.; Ding, C.; Niu, H.; Zhang, T.; Wang, N.; Zhang, Q.; Liu, D.; Han, S.; Yu, H. Effectiveness of crystallitic carbon from coal as milling aid and for hydrogen storage during milling with magnesium. *Fuel* **2013**, *109*, 68–75. [CrossRef]
87. Pal, P.; Agarwal, S.; Tiwari, A.; Ichikawa, T.; Jain, A.; Dixit, A. Improved hydrogen desorption properties of exfoliated graphite and graphene nanoballs modified MgH_2. *Int. J. Hydrogen Energy* **2022**, *47*, 41891–41897. [CrossRef]
88. Rather, S.U.; Taimoor, A.A.; Muhammad, A.; Alhamed, Y.A.; Zaman, S.F.; Ali, A.M. Kinetics of hydrogen adsorption on MgH_2/CNT composite. *Mater. Res. Bull.* **2016**, *77*, 23–28. [CrossRef]
89. Peng, D.; Ding, Z.; Zhang, L.; Fu, Y.; Wang, J.; Li, Y.; Han, S. Remarkable hydrogen storage properties and mechanisms of the shell–core MgH_2@carbon aerogel microspheres. *Int. J. Hydrogen Energy* **2018**, *43*, 3731–3740. [CrossRef]
90. Zhong, Y.; Wan, X.; Ding, Z.; Shaw, L.L. New dehydrogenation pathway of $LiBH_4$ + MgH_2 mixtures enabled by nanoscale LiBH4. *Int. J. Hydrogen Energy* **2016**, *41*, 22104–22117. [CrossRef]
91. Ding, Z.; Shaw, L. Enhancement of Hydrogen Desorption from Nanocomposite Prepared by Ball Milling MgH_2 with In Situ Aerosol Spraying $LiBH_4$. *ACS Sustain. Chem. Eng.* **2019**, *7*, 15064–15072. [CrossRef]
92. Ding, Z.; Li, H.; Shaw, L. New insights into the solid-state hydrogen storage of nanostructured $LiBH_4$-MgH_2 system. *Chem. Eng. J.* **2020**, *385*, 123856. [CrossRef]
93. Ding, Z.; Wu, P.; Shaw, L. Solid-state hydrogen desorption of 2 MgH_2 + $LiBH_4$ nano-mixture: A kinetics mechanism study. *J. Alloys Compd.* **2019**, *806*, 350–360. [CrossRef]
94. Kwak, Y.-J.; Song, M.-Y.; Lee, K.-T. Improvement in the Hydrogen Storage Properties of MgH_2 by Adding NaAlH4. *Metals* **2024**, *14*, 227. [CrossRef]
95. El-Eskandarany, M.S.; Alkandary, A.; Aldakheel, F.; Al-Saidi, M.; Al-Ajmi, F.; Banyan, M. Performance and fuel cell applications of reacted ball-milled MgH_2/5.3 wt% TiH_2 nanocomposite powders. *RSC Adv.* **2018**, *8*, 38175–38185. [CrossRef] [PubMed]
96. Huang, G.; Lu, Y.; Liu, X.; Tang, W.; Li, X.; Wang, F.; Shui, J.; Yu, R. Layered double hydroxide-derived Mg_2Ni/TiH1.5 composite catalysts for enhancing hydrogen storage performance of MgH_2. *J. Magnes. Alloy.* **2023**. [CrossRef]
97. Li, Q.; Guo, Z.; Ding, H.; Jiang, H.; Yang, W.; Du, Y.; Zheng, K.; Huo, L.L. Shaw, MOFs-Based Materials for Sol-id-State Hydrogen Storage: Strategies and Perspectives. *Chem. Eng. J.* **2024**, *485*, 149665. [CrossRef]
98. Shao, H.; Huang, Y.; Guo, H.; Liu, Y.; Guo, Y.; Wang, Y. Thermally stable Ni MOF catalyzed MgH_2 for hydrogen storage. *Int. J. Hydrogen Energy* **2021**, *46*, 37977–37985. [CrossRef]
99. Li, Z.-Y.; Sun, L.-X.; Xu, F.; Luo, Y.-M.; Xia, Y.-P.; Wei, S.; Zhang, C.-C.; Cheng, R.-G.; Ye, C.-F.; Liu, M.-Y.; et al. Modulated noble metal/2D MOF heterostructures for improved hydrogen storage of MgH_2. *Rare Met.* **2023**, *43*, 1672–1685. [CrossRef]
100. Gao, H.; Shi, R.; Shao, Y.; Liu, Y.; Zhu, Y.; Zhang, J.; Li, L. Catalysis derived from flower-like Ni MOF towards the hydrogen storage performance of magnesium hydride. *Int. J. Hydrogen Energy* **2022**, *47*, 9346–9356. [CrossRef]
101. Ma, Z.; Zhang, Q.; Zhu, W.; Khan, D.; Hu, C.; Huang, T.; Ding, W.; Zou, J. Nano Fe and Mg_2Ni derived from TMA-TM (TM = Fe, Ni) MOFs as synergetic catalysts for hydrogen storage in MgH_2. *Sustain. Energy Fuels* **2020**, *4*, 2192–2200. [CrossRef]
102. Grosjean, M.-H.; Zidoune, M.; Roué, L.; Huot, J.; Schulz, R. Effect of ball milling on the corrosion resistance of magnesium in aqueous media. *Electrochim. Acta* **2004**, *49*, 2461–2470. [CrossRef]

103. Park, H.; Jung, C.; Yi, S.; Choi, P.-P. Elucidating the ball-milling-induced crystallization mechanism of amorphous NbCo1.1Sn via atomic-scale compositional analysis. *J. Alloys Compd.* **2023**, *968*, 172014. [CrossRef]
104. Wang, J.; Ebner, A.D.; Ritter, J.A. Kinetic behavior of Ti-doped NaAlH4 when co-doped with carbon nanostructures. *J. Phys. Chem. B* **2006**, *110*, 17353–17358. [CrossRef] [PubMed]
105. Wagemans, R.W.; van Lenthe, J.H.; de Jongh, P.E.; van Dillen, A.J.; de Jong, K.P. Hydrogen Storage in Magnesium Clusters: Quantum Chemical Study. *J. Am. Chem. Soc.* **2005**, *127*, 16675–16680. [CrossRef] [PubMed]
106. Jung, K.S.; Lee, E.Y.; Lee, K.S. Catalytic effects of metal oxide on hydrogen absorption of magnesium metal hydride. *J. Alloys Compd.* **2006**, *421*, 179–184. [CrossRef]
107. Pan, Y.B.; Wu, Y.F.; Li, Q. Modeling and analyzing the hydriding kinetics of Mg-$LaNi_5$ composites by Chou model. *Int. J. Hydrogen Energy* **2011**, *36*, 12892–12901. [CrossRef]
108. Huang, Z.; Guo, Z.; Calka, A.; Wexler, D.; Liu, H. Effects of carbon black, graphite and carbon nanotube additives on hydrogen storage properties of magnesium. *J. Alloys Compd.* **2007**, *427*, 94–100. [CrossRef]
109. Plerdsranoy, P.; Utke, R. Ternary $LiBH_4$–MgH_2–$NaAlH_4$ hydride confined into nanoporous carbon host for reversible hydrogen storage. *J. Phys. Chem. Solids* **2016**, *90*, 80–86. [CrossRef]
110. Lu, Z.; He, J.; Song, M.; Zhang, Y.; Wu, F.; Zheng, J.; Zhang, L.; Chen, L. Bullet-like vanadium-based MOFs as a highly active catalyst for promoting the hydrogen storage property in MgH_2. *Int. J. Miner. Met. Mater.* **2022**, *30*, 44–53. [CrossRef]
111. Ma, Z.; Zou, J.; Khan, D.; Zhu, W.; Hu, C.; Zeng, X.; Ding, W. Preparation and hydrogen storage properties of MgH_2-trimesic acid-TM MOF (TM = Co, Fe) composites. *J. Mater. Sci. Technol.* **2019**, *35*, 2132–2143. [CrossRef]

Disclaimer/Publisher's Note: The statements, opinions and data contained in all publications are solely those of the individual author(s) and contributor(s) and not of MDPI and/or the editor(s). MDPI and/or the editor(s) disclaim responsibility for any injury to people or property resulting from any ideas, methods, instructions or products referred to in the content.